UNLV Theses, Dissertations, Professional Papers, and Capstones

5-1-2016

Effects of Hydraulic Connections on Unsaturated Flow in Dual-Permeability Media

Jeevan Jayakody
University of Nevada, Las Vegas, jeevan.jayakody@gmail.com

EFFECTS OF HYDRAULIC CONNECTIONS ON UNSATURATED FLOW IN DUAL-
PERMEABILITY MEDIA

By

Jeevan Anuradha Jayakody

Bachelor of Science – Geology

University Peradeniya, Sri Lanka

2005

Master of Science – Geoscience

University of Nevada, Las Vegas

2010

A dissertation submitted in partial fulfillment

of the requirements for the

Doctor of Philosophy - Geoscience

Department of Geoscience

College of Sciences

The Graduate College

University of Nevada, Las Vegas

May 2016

Dissertation Approval

The Graduate College
The University of Nevada, Las Vegas

April 21, 2016

This dissertation prepared by

Jeevan Anuradha Jayakody

entitled

Effects of Hydraulic Connections on Unsaturated Flow in Dual-Permeability Media

is approved in partial fulfillment of the requirements for the degree of

Doctor of Philosophy – Geoscience
Department of Geoscience

Michael Nicholl, Ph.D
Examination Committee Chair

Markus Berli, Ph.D.
Examination Committee Member

Elisabeth Hausrath, Ph.D.
Examination Committee Member

Adam Simon, Ph.D.
Examination Committee Member

Dale Devitt, Ph.D.
Graduate College Faculty Representative

Kathryn Hausbeck Korgan, Ph.D.
Graduate College Interim Dean

ii

ABSTRACT

Effects of Morphology of Hydraulic Connections on Inter- and Intra-Matrix Flow in Dual-Permeability Media

by

Jeevan Jayakody

Dr. Michael Nicholl, Examination Committee Chair
Associate Professor of Geoscience
University of Nevada, Las Vegas

A geological medium that exhibits two distinct types of flow is known as dual-permeability medium. Unconsolidated deposits composed of coarse (> 2 mm diameter) clasts (gravel, talus, rockslide debris), engineered systems (heap leach piles, capillary barriers, rock fill), and mine/construction waste fall into this category. The large inter-clast pores that are characteristic of this type of media will drain at near zero matric potentials constraining flow to the interiors of porous clasts and/or the clast surfaces. In either case, water must pass through hydraulic bridges (porous contacts and/or pendular water) that form physical connections between neighboring clasts. Therefore, properties of hydraulic connections place a primary control on flow structure. This dissertation presents three projects designed to study the influence of hydraulic connections on unsaturated flow in dual-permeability media.

A numerical experiment performed to examine how the cross-sectional area and hydraulic conductivity of a bridge influence steady-state flow through a spherical clast is presented in the second chapter of the dissertation. The cross-sectional area of the bridges relative to that of the clast (A_r) was varied across six orders of magnitude between simulations. The ratio of hydraulic conductivity between bridges and clasts (K_b/K_c) was varied across 12

orders of magnitude to consider resistive, neutral, and conductive bridges. Results show a non-linear dependency of volumetric flow through the clast on both A_r and K_b/K_c. The intra-clast flow distribution shifts outwards as A_r increases. Conductive bridges promote this process and resistive bridges impede it.

The third chapter presents a series of bench-scale experiments performed to evaluate the geometry of a pendular bridge under different flow rates through it and at different inclinations. Results show that bridge size increases in a nonlinear fashion with flow rate and decreases with inclination from vertical. The vertical profile of the bridge closely resembled a parabola in all experiments, in contrast to the profile of a static bridge that resembles the arc of a circle. Bridge geometry was independent of flow history. Flow is active through the entire volume of the bridge and exhibits non-laminar characteristics.

The fourth chapter describes a series of bench-scale experiments designed to explore the influence of matrix-to-matrix hydraulic connections on two-dimensional transient wetting of a porous matrix. Cross-sectional area of the connection (A_r) relative to that of the matrix block and location of the connection relative to edges of the block were varied between trials. Results show that the rate of imbibition into the porous block nonlinearly increases with A_r. Moving the connection towards an edge of the block significantly decreases the imbibition rate. Saturation increase of the matrix block before the wetting front reaches all edges remains consistent independent of the connection. The last chapter summarizes results of the research and discusses about future research on this topic.

ACKNOWLEDGEMENTS

First, I thank my advisor, Dr. Michael Nicholl, for his guidance and encouragement to explore the field of unsaturated zone hydrology, which was an entirely new discipline for me before starting graduate studies at UNLV. His enormous support (and patience) allowed me to gain an extensive knowledge on this subject, and develop numerous skills that can be used throughout the rest of my life. I would also like to thank my advisory committee members; Dr. Markus Berli, Dr. Elisabeth Hausrath, Dr. Adam Simon, and Dr. Dale Devitt for their great support for my research. A special thanks goes to Dr. Berli for his assistance in preparing a manuscript from the work presented in the second chapter of this dissertation. I must thank Dr. Ganqing Jiang and Dr. Zhongbo Yu for serving on my comprehensive examination committee with Dr. Nicholl and Dr. Hausrath.

I would like to thank the UNLV Geoscience Department for providing me a graduate assistantship and scholarships during my studies. Also, I highly appreciate the continuous support received from the faculty, staff, and my colleagues in the Geoscience Department. Without their kind assistance, my stay in the department would not have been this enjoyable. I would also like to acknowledge the financial support from the UNLV Graduate and Professional Student Association to purchase equipment for this research. The education that I received from Dr. Jagath Gunatilake, my undergraduate advisor, and the other faculty in the Department of Geology at University of Peradeniya in Sri Lanka is always be remembered.

I am grateful to my friends for their enormous support during my studies. Most of all, I am always thankful to my wife Prabha and daughter Parami for their continuous support and patience, as well as for regularly reminding me my future responsibilities to keep me motivated.

TABLE OF CONTENTS

LIST OF FIGURES

CHAPTER ONE

INTRODUCTION

This dissertation presents numerical and physical experiments designed to investigate the influence of hydraulic connections on unsaturated flow in coarse porous media that is composed of clasts greater than 2 mm in diameter. Porous media in which two distinct flow domains exist; i.e., flow through micro-scale and macro-scale pores, are known as dual-permeability media. Coarse granular media such as gravel deposits, granular soil, and heap leach piles, as well as fractured rocks qualify as dual-permeability media. Water that exists in inter-clast pores in coarse granular media rapidly drains at near-zero matric potentials, restricting water to clast interiors, thin films on clast surfaces, as well as pendular water between narrow spaces and around solid contacts between clasts. Under this condition, pendular water and/or porous contacts that make physical connections between clasts, which are known as hydraulic bridges, facilitate continuity of flow in the medium (e.g., Carminati et al., 2007).

1.1 Chapter 2

The properties of a hydraulic bridge connecting two or more clasts may vary over a wide range. Focusing on a single bridge between two clasts, bridge geometry and conductivity are the key factors that control flow. Previous studies have concluded that volumetric flow through a porous clast with infinitely permeable bridges above and below varies linearly with the cross-sectional area of the bridges (e.g., Carminati et al., 2008; Youngs, 2008). The second chapter of this dissertation presents numerical simulations designed to explore how the cross-sectional area and hydraulic conductivity of bridges influence flow through a spherical clast.

Simulation results show non-linear relationships between volumetric flow rate through the clast (Q) and cross-sectional area of bridges with respect to that of the clast (A_r). Furthermore, data show that Q is very sensitive to the hydraulic conductivity of bridges (K_b) relative that that of the clast (K_c) when $K_b < K_c$, but is relatively insensitive for $K_b > K_c$, Spatial structure of the flow field within the clast and bridges were found to be dependent on both A_r and K_b/K_c. For a constant value of K_b/K_c, spatial distribution of flow in the clast gradually shifts outwards with increasing A_r. Bridges that are more conductive than the clast promote this process, while less conductive bridges impede outwards migration of the flow field. Cross-sectional area is the dominant factor in controlling behavior for $K_b > K_c$, while bridge conductivity is most important for $K_b < K_c$. These results have implications for predictive modeling of flow and solute transport in dual-permeability granular media.

1.2 Chapter 3

Liquid flow on clast surfaces in coarse granular media is expected to occur in the form of films or rivulets. Much like flow through the clast interiors, surface flows must also pass through hydraulic bridges that connect adjoining clasts. Where the clasts are in point-to-point contact, the bridges will consist solely of capillary-held pendular water (i.e., pendular bridges). Since liquid flux, film thickness and fluid pressure in such media are interrelated (e.g., Tokunaga, 2009), we can expect that the surface flux and orientation with respect to gravity will influence the physical properties of a pendular bridge. The literature on pendular bridges mostly concerns isolated bridges, and is quite scarce regarding behavior under flow-through conditions. Because of high conductivity of pendular bridges compared to that of porous contact between clasts, small changes in bridge geometry may significantly alter the macroscopic flow structure in a medium.

Pendular bridges may also be important elements for liquid hold up in granular media. Liquid retention in packed beds of coarse particles increases with fluid flux (e.g., Xiao et al., 2000; Ilankoon and Neethling, 2012). The mechanism for increased retention is not well understood, but can attribute to a combination of pendular bridge volume, film thickness, and/or number of liquid rivulets on the particle surfaces. Therefore, understanding the response of pendular bridges to changing flow conditions is important to predict unsaturated flow and liquid retention in coarse granular media.

The third chapter of this dissertation presents a series of bench-scale experiments that were performed to evaluate the geometry of a pendular bridge under flow-through conditions. Inclination of the bridge with respect to gravity was also considered. The geometry of a pendular bridge formed between two vertical disks in point contact was monitored at different flow rates (Q) and inclinations from the vertical (α). The bridges exhibited a complicated three-dimensional geometry with a smooth transition into the edge films. The size of the bridge increased with Q and decreased with increasing α. At each value of α, width of the bridge increased rapidly at smaller values of Q, and then at a lesser rate at larger values of Q. All observations and measurements were independent of flow history of the system. The meniscus of bridges formed under flowing conditions closely resembled a parabola while those formed under non-flowing conditions followed the arc of a circle. Minor temporal fluctuations in film thickness on the disc surfaces correlated strongly with measurable changes in bridge size. These results show that spatial and temporal variability in local fluid flux, as well as the distribution of orientation of inter-clast contacts should be considered when characterizing the macro-scale flow structure in coarse granular media.

1.3 Chapter 4

The first two parts of this dissertation considered hydraulic bridges under steady-state conditions where flow is driven by gravity. Capillary forces are expected to play an important role in the transient wetting of porous clasts. For capillary-driven slow flow into initially dry clasts (imbibition), advancement of the wetting front will depend on the formation of hydraulic connections (bridges) where none previously existed. Mass flow across such connections is expected to depend highly on the cross-sectional area. The need to vary the area of a hydraulic connection between experiments to evaluate its effects on imbibition makes physical experiments of this scale infeasible, because micro-scale heterogeneities of the connection can significantly affect the system behavior. Furthermore, precisely monitoring the flow into a single clast (Carminati and Fluehler, 2009) is very challenging. Therefore, employing bench-scale experiments, where imbibition can be easily observed under various, well-defined hydraulic connections is more practicable. Since all other properties of the flow system remain consistent between experiments, this approach will helps to clearly understand the influence of hydraulic connections on imbibition. Furthermore, knowledge acquired from bench-scale flow system can be also applied for imbibition in fractured porous media. Similar to drainage of inter-clast pores in coarse granular media, relatively wide apertures in fractured rocks also drain at near-zero matric potentials (e.g., Wang and Narasimhan, 1985). Matrix to matrix contacts points and/or liquid bridges formed due to spatial heterogeneity within a fracture aperture create local hydraulic connections to facilitate inter-block flow (e.g., Peters and Klavetter, 1988; Glass et al., 1995; Seol et al., 2003).

The fourth chapter of the dissertation presents a series of bench-scale experiments that were conducted to explore the influence of inter-block hydraulic connections on capillary-driven,

two-dimensional flow between adjoining matrix blocks. The physical system consisted of one saturated sandstone block that was instantaneously placed in contact with a dry block of the same material. We considered the effects of: (i) the cross-sectional area (A) of the connection relative to that of the block, and (ii) the position of the connection relative to edges of the blocks on imbibition into the dry block. The rate of imbibition varied with both A and the location of the inter-block connection. At A = 100%, measured imbibition was comparable to 1D absorption-based predictions, but deviated substantially as A decreased. At constant A, the imbibition rate decreased as the inter-block contact shifted closer to edges of the block. For all values of A, and positions of the connection, imbibition rate decreased significantly as the wetting front reached the edges of the block. Saturation (S) of the block at this stage (0.48 ± 0.02) was insensitive to A or location of the connection. Results show that the hydraulic connections place a first-order control on the evolution of flow fields in both coarse granular media and fractured rocks. The observed relationships may be incorporated into continuum-based models to improve predictions of unsaturated flow and solute transport.

CHAPTER 2

INFLUENCE OF HYDRAULIC BRIDGES ON FLOW WITHIN COARSE POROUS CLASTS

2.1 Abstract

Unsaturated flow in coarse granular media is controlled by inter-clast hydraulic bridges. Previous studies suggest that volumetric flow through a porous clast (Q) will be linearly dependent on the cross-sectional area of the hydraulic bridges, and understate the importance bridge conductivity. Numerical simulations were performed to explore steady-state flow through a spherical clast with identical bridges located at the top and bottom. The cross-sectional area of the bridges relative to that of the clast (A_r) was varied across six orders of magnitude. The ratio of hydraulic conductivity between bridges and clasts (K_b/K_c) was varied across 12 orders of magnitude to consider resistive, neutral, and conductive bridges. Results show a non-linear dependency of Q on both A_r and K_b/K_c. The intra-clast flow distribution shifts outwards as A_r increases. Conductive bridges promote this process and resistive bridges impede it.

2.2 Introduction

Conventional concepts of capillary dominated unsaturated flow (e.g., Richards, 1931; Philip, 1957a) do not transfer well to media composed of coarse (> 2 mm diameter) clasts, such as unconsolidated gravel deposits, granular soil, heap leach piles, engineered capillary barriers, and mine/construction waste. In contrast to the pore-filling behavior observed in fine-grained materials, inter-clast pores in coarse media drain at near zero matric potentials, thus constraining mobile water to clast interiors, surface films, and pendular water that connects adjoining clasts (e.g., El Boushi and Davis, 1969; Tokunaga et al., 2003). In the absence of airborne transport

mechanisms (i.e., dripping and vapor phase flow), unsaturated flow in such media must move either on the surface of clasts, or through the permeable interior of the clasts (intra-clast flow). For both surface and intra-clast flow, water must pass through hydraulic bridges (i.e., porous contacts and/or pendular water) that form physical connections (Figure 2.1) between adjoining clasts (Hu et al., 2004; Carminati, Kaestner, Ippisch et al., 2007). As a result, hydraulic bridges place an important control on flow, solute transport, and geochemical processes. In this study, we neglect surface flow to consider the influence of hydraulic bridges on intra-clast flow.

The materials that comprise a hydraulic bridge will be some combination of porous media, impermeable solid, and/or pendular water that physically connects two adjacent clasts (Tokunaga et al., 2003; Carminati et al., 2007; Berli et al., 2008). The geometry and hydraulic conductivity (K) of those materials are expected to play important roles in determining behavior of the bridge. Although the three-dimensional geometry of a hydraulic bridge may be quite complicated, it is expected that the cross-sectional area perpendicular to flow will be no larger, and perhaps much smaller than that of the adjoining clasts (e.g., Figure 2.1). Therefore, the flow field within the clasts must narrow to pass through the bridge, increasing resistance by inducing longer flow paths and creating locally steep gradients near the constriction (Youngs, 2008). Thickness of the bridge is likely to vary in space (Carminati et al., 2007), with an effect that depends on the hydraulic conductivity of the bridge materials (K_b) relative to that of the clast materials (K_c). Pendular water (Figure 2.1) is expected to offer little resistance to flow and produce a "conductive bridge" ($K_b > K_c$) that funnels flow into thicker portions of the bridge. Conversely, a "resistive bridge" ($K_b < K_c$) might form where a porous contact contains either large pores that drain at the in situ fluid pressure (Carminati et al., 2008) or a significant amount of impermeable materials (e.g., mineral precipitates). Resistive bridges are likely to divert flow

7

away from localities where the bridge is thicker. A "neutral bridge" ($K_b \approx K_c$) with hydraulic properties roughly equivalent to the clast (e.g., extensive matrix-matrix contact) will impact flow solely by imposing a physical constriction.

Figure 2.1: A hydraulic bridge connecting two sandstone clasts. Both clasts are rigid and no confining pressure has been applied (negligible deformation at the contact). As a result, the bridge consists primarily of pendular water surrounding a point contact.

Relatively few investigations have considered the influence of hydraulic bridges on intra-clast flow. Carminati et al. (2007, 2008) used x-ray and neutron radiography to characterize time-variant unsaturated flow through vertically stacked soil clasts (aggregates). Hydraulic bridges in these experiments were composed of unstrained matrix-matrix contacts and pendular water. Results suggested that the cross-sectional area of the bridges places a first-order control on both volumetric flow and the distribution of moisture within the system. Use of bridge cross-sectional area as a calibration parameter led to a close match between experimental results and

numerical simulations. In those simulations, the bridges were assumed to be of uniform thickness and conductivity. Youngs (2008) considered saturated flow through a spherical clast of radius R_c with infinitesimally thin polar end caps of radius R_b held as constant head boundaries, and no flow boundaries elsewhere on the surface. Analogy to electric flux through a disk of radius R_b located on the surface of an infinite half-space led to the following estimate for volumetric flow (Q) through the sphere:

$$Q = 4KR_b\Delta h \qquad \text{Eq. (2.1)}$$

where K represents the hydraulic conductivity of the half-space, and Δh is the head difference between the disk and boundaries of the half-space at infinity. Predictions based on Eq. (2.1) were reported to be in close agreement with numerical simulations and an analog electrical model for values of R_b/R_c between ~0.03 and 0.15.

In this study, we build on the work of Youngs (2008) to better understand how hydraulic bridges control intra-clast flow at the scale of an individual clast. Given the difficulty of isolating the effects of bridges in physical experiments, we employ detailed numerical simulations to characterize volumetric flow and the spatial distribution of flow through a single spherical clast as a function of size and conductivity of the bridges. To maintain our focus on hydraulic bridges, we hold the size, shape, and hydraulic conductivity of the clasts constant. The cross-sectional area of the bridges relative to that of the clast (A_r) is varied across six orders of magnitude (10^{-6} to 10^0). The hydraulic conductivity of the bridges is varied across 12 orders of magnitude to consider conditions ranging from highly resistive ($K_b/K_c = 10^{-6}$) to highly conductive ($K_b/K_c = 10^6$). Results show that hydraulic bridges place a first order control on both volumetric flux between clasts, and the distribution of flux within the clasts. For neutral and conductive bridges

($K_b/K_c \geq 1$), A_r is found to be the dominant factor in determining volumetric flow, while K_b/K_c is the primary control for resistive bridges ($K_b/K_c < 1$).

2.3 Conceptualization and Numerical Approach

The influence of hydraulic bridges on intra-clast flow is considered by defining a single undeformed spherical clast (e.g., Bartlett, 1997; Ghezzehei and Or, 2000; Youngs, 2008) of radius R_c (> 1 mm) that is connected to the surrounding flow field solely through hydraulic bridges located at the top and bottom (Figure 2.2a). Steady-state flow is assumed to occur only within the interior of the permeable clast and the bridges (i.e., no surface flow). Following Youngs (2008), hydraulic conductivity of the clast (K_c) is assumed to be spatially uniform and isotropic. The hydraulic bridges are treated as cylinders of radius R_b that connect smoothly with the spherical clast, and exhibit a uniform hydraulic conductivity (K_b). It is further assumed that K_c, K_b, and R_b are independent of fluid pressure in the clast. Presuming identical clasts above and below (not shown in Figure 2.2a), we take the horizontal plane through the center of each bridge to be an equipotential surface. The difference of total head (h) between the two bridges is taken to be the difference in elevation above datum (z = 0). Under the stated conditions, flow will be driven solely by the gravitational component of the gradient (dh/dz = 1), and is fully described by the three-dimensional Laplace equation (e.g., Bear, 1988).
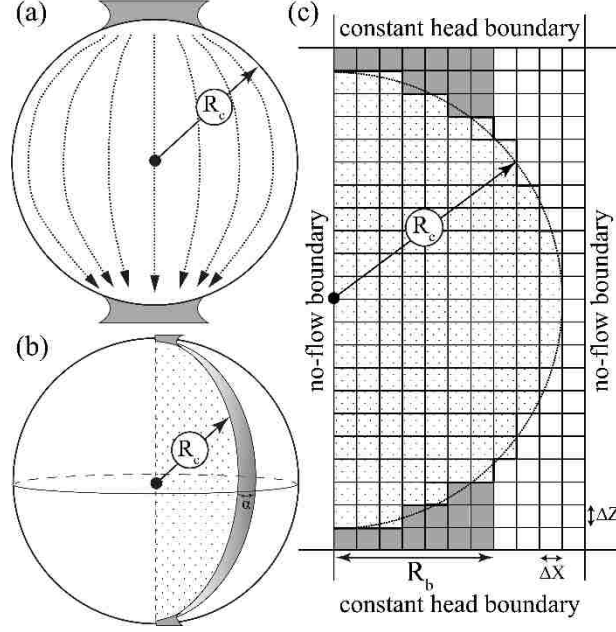
Figure 2.2: (a) Vertical section through a spherical clast with hydraulic bridges (gray) at the top and bottom. Dotted arrows show hypothetical flow lines within the permeable matrix. (b) Numerical simulations were performed on a narrow wedge (shaded region) of dihedral angle α that passes through both the clast and bridge. (c) The wedge shown in Figure 2.2b is projected onto a two-dimensional finite-difference grid. Radius of the clast is R_c and the radius of the bridges is R_b. Individual grid blocks ($\Delta x = \Delta z$) are categorized as hydraulic bridge (gray), porous solid (dotted) or surrounding air (unshaded).

Rather than solving the Laplace equation for steady flow through the entire three-dimensional system described above, we focus on a narrow wedge (Figure 2.2b) that is defined by two vertical half-disks separated by a small dihedral angle ($\alpha = 1°$). From radial symmetry about the vertical axis, flux in the wedge will be representative of that in the system as a whole. For both clast and bridge, the component of flow in the direction of α will be small compared to that in the plane of the half-disks, and thus can be assumed as negligible. This simplification allows us to use the two-dimensional Laplace equation with space-variant transmissivity to approximate three-dimensional flow in the narrow wedge:

$$T_x \frac{\partial^2 h}{\partial x^2} + T_z \frac{\partial^2 h}{\partial z^2} = 0 \qquad \text{Eq. (2.2)}$$

11

where T_x and T_z represent transmissivity in the horizontal and vertical directions, respectively. Local transmissivity values are defined as the product of hydraulic conductivity (K_c or K_b) and thickness of the wedge (d), which is a function of α and horizontal distance from the vertical axis of the clast.

The block-centered finite difference form of Eq. (2.2) is solved for h on a two-dimensional rectangular grid (Figure 2.2c) through Gauss-Seidel iteration (e.g., Press et al., 1986). The top and bottom edges of the grid are defined as constant head boundaries (unit downwards gradient), with no-flow boundaries along the left- and right-hand edges. Hydraulic conductivity of individual grid blocks is assigned based on whether the center of the block lies within the clast (K_c), bridge (K_b), or in the surrounding air (K_a). Effective transmissivity between neighboring grid blocks is taken to be the harmonic mean of the individual values (e.g., Bear, 1988). High-resolution grids with $> 2 \text{ x} 10^6$ nodes ($R_c = 1000$ grid blocks) are used to minimize the effects of approximating the spherical clast with square blocks. A very small value was assigned to K_a to improve numerical stability of the solution at little cost to accuracy. The numerical code was validated against one-dimensional Darcy flow in a cylinder ($K_b = K_c$, $R_b = R_c$) and an analytical solution presented by Wheatcraft and Winterberg (1985) for two-dimensional flow through a circular slab embedded in a second material ($K_b \neq K_c$, $R_b \gg R_c$, d = constant). The minimum thickness of the bridge was arbitrarily set to one grid block ($R_c/1000$) as shown in Figure 2.2c, and held constant for all simulations.

2.4 Simulation Results

Simulations were conducted to explore the influence of hydraulic bridges on: 1) volumetric flow (Q) at unit hydraulic gradient; and 2) the spatial distribution of flow within the

clast and bridges. Input parameters were non-dimensionalized by scaling to the hydraulic conductivity (i.e., K_b/K_c, K_a/K_c) or radius (i.e., R_b/R_c, x/R_c, z/R_c, h/R_c) of the clast. Hydraulic conductivity of the bridges relative to that of the clast (K_b/K_c) was varied over a broad range of arbitrary values to consider resistive ($K_b/K_c = 10^{-6}$, 10^{-3}), neutral ($K_b/K_c = 10^0$), and conductive ($K_b/K_c = 10^3$, 10^6) bridges. For all simulations, the relative conductivity of the air surrounding the clast (K_a/K_c) was held constant at 10^{-9}. The cross-sectional area of the bridge relative to that of the clast was parameterized as $A_r = R_b^2/R_c^2$ and varied incrementally from 10^{-6} to 10^0 at each value of K_b/K_c. Volumetric flow through the clast is reported in non-dimensional form as Q/Q_d, where Q_d represents unit-gradient flow at $K_b/K_c = 1$ and $A_r = 1$ (i.e., a cylinder of radius R_c and conductivity of K_c).

Simulation results (Figure 2.3) for the neutral and conductive bridges ($K_b/K_c \geq 1$ differed substantially from those for the resistive bridges ($K_b/K_c < 1$). Looking first at the neutral/conductive bridges ($K_b/K_c = 10^0$, 10^3, 10^6 in Figure 2.3), flow was controlled almost entirely by A_r, and was relatively insensitive to K_b/K_c for $A_r < 6.4 \times 10^{-1}$ (i.e., $R_b/R_c = 0.8$). For both types of bridges, flow varied by >3 orders of magnitude over six orders of magnitude change in A_r. The differences in Q/Q_d associated with K_b/K_c are most pronounced for the end member case of $A_r = 10^0$. Results can be broken down into three regimes based on the shape of Q/Q_d vs. A_r plot. At small A_r ($< 10^{-4}$), the functional form of the data is concave downwards. Data for the two conductive bridges ($K_b/K_c = 10^3$, 10^6) are nearly coincident, and plot slightly above those for the neutral bridge ($K_b/K_c = 10^0$) with the maximum difference at the smallest value of A_r. At intermediate values of A_r (10^{-4} to 10^{-1}), values of Q/Q_d are nearly independent of K_b/K_c, and follow an approximately linear trend in log-log space with a slope of slightly less than $A_r^{0.5}$. At the largest values of A_r ($> 10^{-1}$), all three data sets are concave upwards. Data for the

13

two conductive bridges remain coincident until A_r reaches $\sim 6.4 \times 10^{-1}$, where both start to

increase sharply. As expected, Q/Q_d for the neutral bridge gradually increases to reach 10^0 at A_r

$= 10^0$ (i.e., a homogenous cylinder).
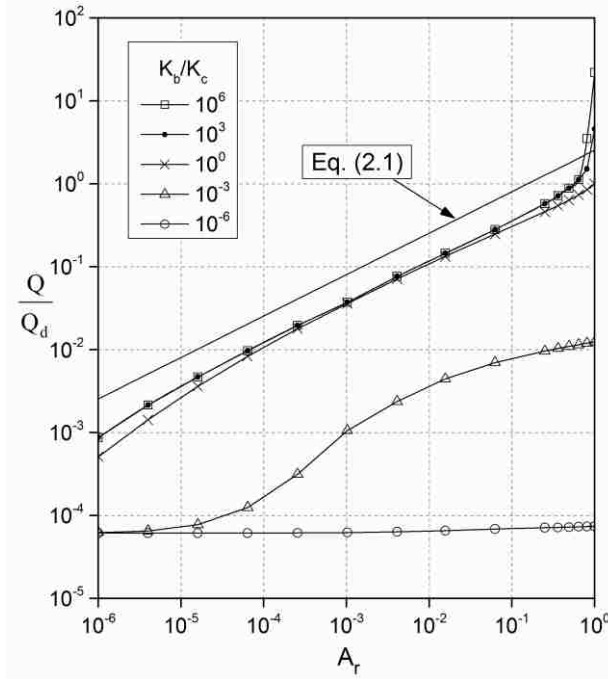
Figure 2.3: Volumetric flow through the clast (Q) relative to unit gradient flow (Q_d) through a cylinder of radius R_c and conductivity K_c is shown as a function of A_r for different values of K_b/K_c. Predictions based on Eq. (2.1) are shown for comparison.

In contrast to the results for the neutral/conductive bridges, the sensitivity of flow to A_r

for the resistive bridges ($K_b/K_c = 10^{-3}$, 10^{-6} in Figure 2.3) showed a high degree of dependency

on K_b/K_c. Values of Q/Q_d for the resistive bridges converged at small A_r ($< 10^{-5}$), then separated

by more than two orders of magnitude as A_r increased. Over the six orders of magnitude change

in A_r, Q/Q_d varied by two orders of magnitude for $K_b/K_c = 10^{-3}$ and negligibly for $K_b/K_c = 10^{-6}$.

The reduction in Q/Q_d from the neutral bridge to the resistive bridges increased with A_r and

covered a range of 1-4 orders of magnitude. Both sets of results for resistive bridges follow an S-

shaped curve that lacks the broad linear feature apparent in simulations for the

14

neutral/conductive bridges and curves in the opposite direction; i.e., concave upwards at small A_r ($< 10^{-3}$) and downwards at larger A_r.

Properties of the bridges (K_b/K_c, A_r) have a substantial effect on the spatial distribution of flow within the clast (Figure 2.4). The effects are most apparent close to the bridge, and become small near the equatorial plane of the clast, which is an equipotential line from symmetry (i.e., flow lines must cross at a right angle). At the smallest value of A_r that we considered (10^{-6}), the spatial distribution of flow was nearly the same for all values of K_b/K_c (Figure 2.4a is presented as an illustrative example). Flow lines enter the clast through a narrow region, diverge in the upstream half of the clast to distribute flow, and then converge in the downstream half of the clast to exit again through a narrow region. As A_r increases, flow lines shift towards the outside of the clast/bridge (see illustrative examples in Figure 2.4b-d). For the resistive bridges, the separation between flow lines increases away from the center of the clast (Figure 2.4b), while the opposite happens for the neutral and conductive bridges (Figures 2.4c, d). As K_b/K_c increases, the flow lines shift further towards the outside of the bridge and become increasingly close together at the perimeter. Where $K_b \neq K_c$, flow lines refract at the clast-bridge interface to increase the cross-sectional area in the less permeable material (Figure 2.4b, d). With the neutral bridge, there is no refraction of flow lines when they cross into the clast (Figure 2.4c). However, the flow lines bend a short distance into the clast to accommodate the change in cross-sectional area within the clast.
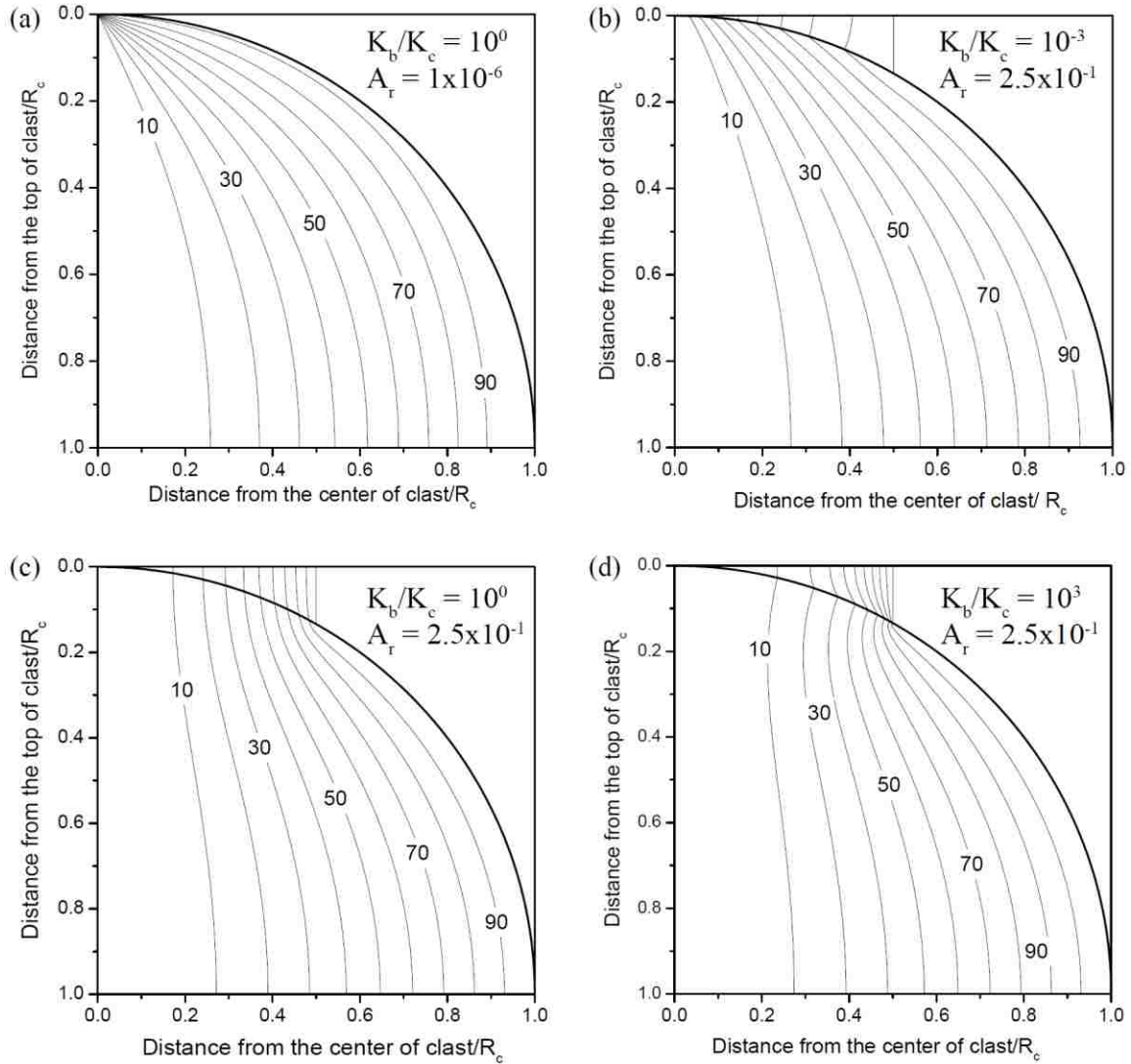
Figure 2.4: Illustrative examples showing the distribution of flow in the upper bridge and clast; the lower half of the system is a mirror image of the upper half. The vertical axis of rotation is treated as zero flow, and each successive flow line represents an additional 10% of the total flow (labeled 10-90%). The outer edge of the clast/bridge encloses 100% of the flow. In three dimensions, each flow line would be rotated through 360˚ around the vertical axis to create a surface; thus a unit area near the outside of the cross section corresponds to a much larger fraction of the sphere volume than one near the axis of rotation.

The spatial distribution of flow (Figure 2.4) suggests that small values of A_r and/or K_b/K_c will tend to focus head loss within, and in the vicinity of the bridges. To illustrate this effect, Figure 2.5 shows the average vertical distance (L/R_c) between the upper boundary of the upstream bridge (h = $2R_c$) and the equipotential surface for h = $1.1R_c$, which represents 90% of

16

the head loss in the upper half of the system (clast and bridge). For small bridges ($A_r < 10^{-4}$), the

spatial distribution of head loss is independent of K_b/K_c and occurs both within, and very close to

the bridges. As A_r increases, depth to the $1.1R_c$ equipotential surface rapidly increases for the

neutral and conductive bridges. For these bridges, variation in the depth of the $1.1R_c$

equipotential surface increases with A_r, and then decreases as A_r approaches 10^0. At $A_r = 10^0$, the

neutral bridge forms a uniform cylinder with horizontal equipotential lines. In contrast, the depth

to the $1.1R_c$ equipotential surface does not considerably change for the resistive bridges until A_r

$> 10^{-1}$, which shows the dominant effect of low hydraulic conductivity of resistive bridges on

flow.
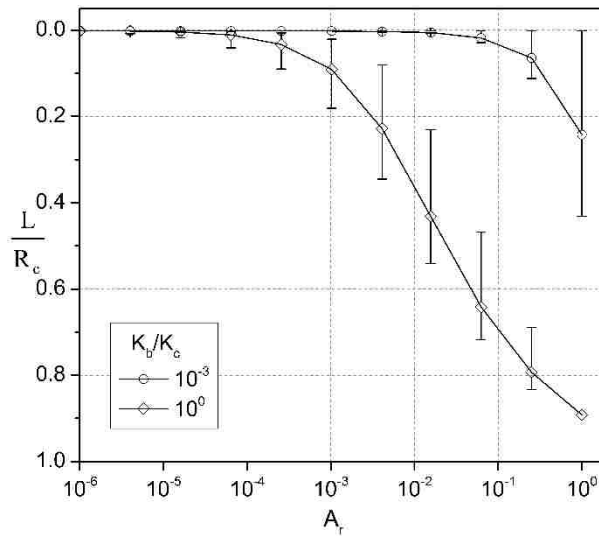
Figure 2.5: Average depth (L/R_c) from the upper boundary of the upstream bridge to the $1.1R_c$ equipotential line (head loss of $0.9R_c$) is shown as a function of A_r. Error bars show the range of depths. Note that $L/R_c = 1.0$ represents the equatorial plane of the clast. For clarity, only the neutral bridge and one resistive bridge are shown. Data for the conductive bridges (not shown) nearly coincides with that for the neutral bridge when $A_r < 10^{-2}$, and plot slightly below (i.e., depth increases compared to that for the neutral bridge) when $A_r > 10^{-2}$.

2.5 Discussion

Simulation results show that flow in our idealized system (Figure 2.2) exhibits a nonlinear dependence on both the relative size (A_r) and conductivity (K_b/K_c) of the bridges (Figures 2.3 - 2.5). At the smallest value of A_r that we considered (10^{-6}), the distribution of flow (Figure 2.4a) is independent of K_b/K_c, with most head loss occurring in the bridge or immediate vicinity (Figure 2.5). Flow fields at small A_r are consistent with predictions based on an analytical solution for heat flow between a point source and a point sink ($A_r \to 0$, $K_b/K_c \to \infty$) located at the opposite poles of a homogeneous solid sphere (Youngs and Kacimov, 2007). For this situation, the effective transmissivity of the clast is controlled by the structure of the internal flow field, which is independent of K_b/K_c. Thus, volumetric flow is controlled by the conductivity of the bridge, with Q/Q_d displaying an apparent limiting behavior as K_b/K_c increases or decreases (Figure 2.3). The effective transmissivity of the system will be given by the weighted harmonic mean of transmissivities for the clast and bridges Bear, 1988. Thus, at small A_r, the limit on effective transmissivity will be primarily controlled by the lesser of the two transmissivities and the thickness of the bridges relative to that of the clast.

As A_r increases, flow shifts towards the outside of the clast, causing the average path length within the clast to decrease. The degree to which the flow paths shift depends heavily on K_b/K_c (Figures 2.4b-d). Given the geometry of our conceptual model (Figure 2.2), both the thickness and cross-sectional area of the bridges increase with distance from the vertical axis of the clast. For conductive bridges, increased thickness and area both act to enhance flux, causing flow paths within the clast to migrate outwards. As A_r gets large ($> 1 \times 10^{-1}$), the minimum

18

distance between the upper and lower bridges decreases rapidly. For conductive bridges, this creates highly efficient flow paths towards the outside edges of the clast and leads to a rapid increase in Q/Q_d as A_r approaches 10^0 (Figure 2.3). In contrast, increased thickness and cross-sectional area have opposing effects for resistive bridges, as the former acts to inhibit flow. For the situations considered here ($K_b << K_c$), low conductivity overwhelms the increased cross-sectional area with increasing A_r and restricts outwards migration of flow paths within the clast (Figure 2.4b). For the neutral bridge ($K_b = K_c$), increased bridge thickness is irrelevant, and flow paths move towards the outside of the clast solely due to the increased cross-sectional area of flow.

The model suggested by Youngs (2008) and presented above as Eq. (2.1) gives values of Q/Q_d that plot as a straight line in log-log space with a slope of $A_r^{0.5}$ (Figure 2.3). This model over-predicts our simulation results for the most conductive bridge ($K_b/K_c = 10^6$) by a factor of 2-3 for $A_r < 6.4 \times 10^{-1}$ and does not display any of the curvature found in all of our results. Youngs' model is based on an assumption that a spherical clast with a bridge of small A_r can be represented by a circular constant head boundary located on the surface of an infinite half-space. Our conceptual model (Figure 2.2) differs in that: 1) our constant head boundaries are not located directly on the surface of the clast, thus allowing head loss and lateral diversion within the bridge; and 2) flow within our clast is confined to a finite sphere rather than an infinite half-space. Looking first at point (1), for $A_r < 6.4 \times 10^{-1}$ our simulation results (Figure 2.3) appear to rapidly converge with increasing K_b/K_c. This observation strongly suggests that our conductive bridges closely mimic a constant head boundary on the surface of the clast and are thus consistent with Youngs' assumption. It is more likely that the observed discrepancy between Youngs' model and our results can be attributed to point (2), which reflects a basic difference in

system geometry. Youngs (2008) assumed that as $A_r \to 0$, curvature of the clast in the immediate

vicinity of the bridge is small, and thus resembles a point source located on a flat surface (i.e.,

infinite half-space). This approach neglects the finite volume of the spherical clast, which

reduces the cross-sectional area available for flow (with respect to infinite space) leading Eq.

(2.1) to overestimate Q/Q_d.

We compared our simulation results to other models from the literature and some obvious

approximations (Figure 2.6). We chose to make the comparison at $K_b/K_c = 10^0$ (neutral bridge)

because an analytical solution exists at $A_r = 10^0$ (i.e., $Q/Q_d = 10^0$). Carminati et al. (2008)

suggested that an effective hydraulic conductivity for a clast-bridge system could be defined as:

$$K_{eq} = K_c \, A_r \qquad\qquad \text{Eq. (2.3)}$$

In effect, this approach treats the system as a cylinder with the conductivity of the clast

and diameter of the bridge. At small A_r, this model under-predicts our simulation results by

several orders of magnitude, but is in closer agreement at large A_r, where system geometry

approaches that of a cylinder. This model would be most appropriate for clasts that are elongated

perpendicular to flow and have a large A_r. Assuming vertical flow through a series of horizontal

layers Carminati et al., 2007, an equivalent transmissivity for one-dimensional flow (T_{eq}) can be

calculated as:

$$T_{eq} = \left(\sum_{j=1}^{m} 1 / \left(\sum_{i=1}^{n} T_{i,j} \right) \right)^{-1} \qquad\qquad \text{Eq. (2.4)}$$

where $T_{i,j}$ is transmissivity of the ith grid block (column) in the jth row, m is the number of rows

and n is the number of columns in the two-dimensional finite difference grid (Figure 2.2c).

Predictions based on Eq. (2.4) over-estimate our simulations by a factor of 2-7 for $A_r < 6 \times 10^{-2}$,

but provide better results for both smaller and larger bridges. Finally, we simulated flow on the

finite difference grid by solving Eq. (2.2) with d held constant (i.e., a two-dimensional slab rather

than a wedge). This approach over-predicts flow by two orders of magnitude at small A_r, and more closely reflects predictions based on wedge geometry for $A_r > 6$ x 10^{-2}. The over-prediction at small A_r is primarily due to overestimation of local transmissivity close to the vertical axis, which tends to focus flow along the center of the clast/bridge rather than distributing it laterally. This last result confirms the importance of accounting for three-dimensional geometry of the system.
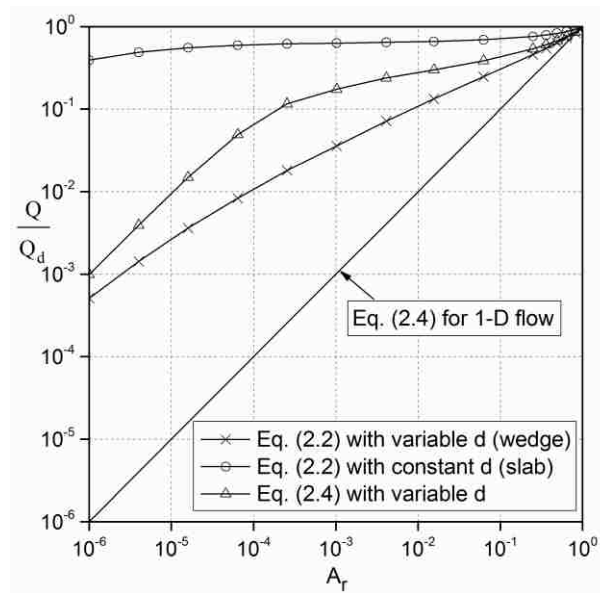
Figure 2.6: Volumetric flow through a spherical clast approximated using different numerical methods as a function of A_r. For all methods, $K_b/K_c = 10^0$.

In media where the clasts are semi-spherical in shape, bridges composed primarily of pendular water are expected to be considerably smaller than the clasts ($A_r < 1$). In real systems, sub-spherical clasts are likely to connect to their neighbors through multiple bridges. As A_r increases, these adjoining bridges would likely merge to induce inter-clast flow. In addition, the stability of liquid bridges with respect to gravity will decrease rapidly for $R_c > 2$ mm (Saez and Carbonell, 1990) precluding large values of A_r. For these reasons, $A_r < 2.5$ x 10^{-1} (i.e., $R_b/R_c < 0.5$) would appear to be a reasonable range to find in real systems. The actual size of purely

liquid bridges can be related to fluid pressure provided that clast size, geometry and surface chemistry are known (Reinson et al., 2005; Bear et al., 2011). The hydraulic conductivity of the liquid bridges could then be estimated from Poiseuille's Law by treating the bridges as capillary tubes of radius R_b. Real liquid bridges would likely be of larger diameter than pores in the clast, resulting in $K_b/K_c > 10^0$. Since our results (Figure 2.3) show that the influence of K_b is small for neutral and conductive bridges, this parameter could be treated as a constant rather than calculated as a function of A_r.

The geometry and hydraulic conductivity of porous bridges will be affected by local clast geometry, deformation, fluid pressure, and geochemical activity (e.g., precipitation, dissolution). In contrast to liquid bridges, the size of porous bridges formed through deformation or precipitation at the contact may approach $A_r = 10^0$. The hydraulic properties of porous bridges formed through direct inter-clast contacts (Ghezzehei and Or, 2000; Hu et al., 2004) and/or meniscus-type precipitation of minerals in inter-clast pores (Badiozamani et al., 1977) will change by orders of magnitude with fluid pressure (Carminati et al., 2007) and compaction (Berli et al., 2008). As such, porous bridges may behave similar to the conductive, neutral, or resistive bridges described above.

2.6 Conclusions

Numerical simulations were employed to consider gravity-driven flow through a spherical clast bound by two hydraulic bridges. Results show that both relative cross-sectional area (A_r) and hydraulic conductivity (K_b/K_c) of the bridges influence volumetric flow (Q/Q_d) through the clast, as well as the distribution of flow within the clast. In contrast to previous studies (Carminati et al., 2008; Youngs, 2008), Q/Q_d was found to exhibit a non-linear

dependence on A_r at all values of K_b/K_c that were considered. For the neutral ($K_b/K_c = 1$), and conductive ($K_b/K_c > 1$) bridges, the value of Q/Q_d is controlled by A_r, and is relatively insensitive to K_b/K_c. In contrast, K_b/K_c imposes the primary control on Q/Q_d for resistive ($K_b/K_c < 1$) bridges, and A_r has a secondary, but still significant effect. For all cases, the intra-clast flow field expands outwards as A_r increases, displaying the largest change in the vicinity of bridges. However, outward expansion of the flow field is highly influenced by the value of K_b/K_c in that conductive bridges promote outward expansion of the flow field, while resistive bridges hinder expansion.

Results of this study can be used to evaluate flow, geochemical interactions between clasts and water, as well as solute transport in granular soil and unconsolidated granular media when surface flow is negligible. Simulated flow data show that different combinations of hydraulic conductivity and cross sectional area of bridges can produce the same volumetric flow rate through a clast, but the spatial structure of intra-clast flow field will be different between those cases. Identifying such differences is important in evaluating flow, solute transport and geochemical processes in unsaturated granular media.

CHAPTER 3

GEOMETRY OF PENDULAR BRIDGES: EFFECTS OF FLOW RATE AND GRAVITY

3.1 Abstract

Pendular bridges provide hydraulic connections between neighboring clasts, and operate as elements for liquid retention under unsaturated flow conditions in coarse granular media. Therefore, understanding how pendular bridges interact with film flow on the clast surfaces is an important prerequisite to understanding flow in this type of media. Experiments were designed to collect quantitative data from a single pendular bridge located at the contact between two vertical discs. Geometry of the bridge was measured as a function of volumetric flow through the bridge and inclination with respect to gravity. Results show that bridge size increases in a nonlinear fashion with flow rate and decreases with inclination from vertical. Increases in bridge area correlate strongly with increased radius of the air-water meniscus, suggesting that fluid pressure in the bridge becomes less negative with increasing flow. The vertical profile of the bridge closely resembled a parabola in all experiments. This contrasts with static (non-flowing) bridges in the same apparatus, where the bridge profile resembled the arc of a circle. Bridge geometry was observed to be independent of flow history (flow rate and inclination), and rapidly adjusts to changing flow conditions. Flow is active through the entire volume of the bridge and the internal flow field exhibits non-laminar characteristics.

3.2 Introduction

Pendular water that connects neighboring clasts plays an important role in controlling unsaturated flow through coarse (> 2 mm diameter) granular media such as: natural gravels,

24

construction debris, mine waste, heap leach pads, trickle-bed reactors, and engineered capillary

barriers. The large inter-clast pores that are characteristic of such media will drain at near zero

matric potentials, thus constraining flow to the interiors of porous clasts and/or the clast surfaces.

In either case, all flow must pass from clast-to-clast through some form of hydraulic connection

or bridge. Here, we ignore porous connections (e.g., Berli et al., 2008) to focus on bridges that

occur where pendular water is trapped between adjoining clasts (e.g., Turner and Hewitt, 1959;

Conca and Wright, 1992; Tokunaga, 2009). Unlike porous bridges, the hydraulic conductivity of

pendular bridges will be independent of fluid pressure and quite high. Conversely, bridge size

and hence transmissivity along the flow path will likely be sensitive to fluid pressure (e.g.,

Carminati et al., 2008). In addition, pendular bridges will facilitate mixing, and may be

ephemeral features under transient conditions. For these reasons, the hydraulic behavior of

pendular bridges is likely to be inconsistent with standard conceptual models for unsaturated

flow and needs to be considered through experiment.

Static pendular bridges (i.e., no internal flow) have been studied extensively in the

context of inter-granular forces due to capillary pressure (e.g., Willett et al., 2000; Slobozhanin

et al., 2006; Mielniczuk et al., 2014) and liquid holdup (retention) between spherical clasts (e.g.,

Kramer, 1998; Lu et al., 2008). In the case of static pendular water connecting two hydrophilic

clasts (Figure 3.1), capillary forces along the contact lines place the bridge under tension. The

pressure difference across the air-water interface (ΔP) is then given by the Young-Laplace

equation:

$$\Delta P = \gamma \left(\frac{1}{R_1} + \frac{1}{R_2} \right) \qquad \text{Eq. (3.1)}$$

where γ is surface tension, and the term in parentheses represents the local mean curvature of the

meniscus (e.g., Bear, 1988). As drawn in Figure 3.1, the two principal radii of the meniscus R_1

and R_2 have opposite signs, with a negative resultant (mean curvature) required for fluid pressure in the pendular bridge to be sub-atmospheric.
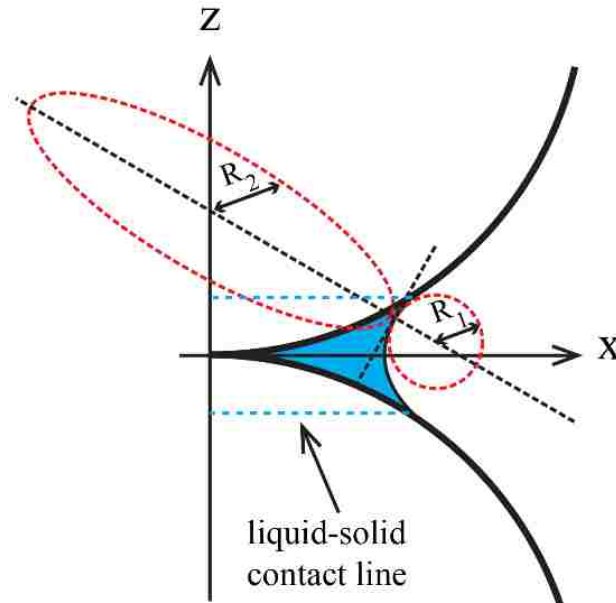
Figure 3.1: Two-dimensional illustration of a static pendular bridge between two curved solid surfaces. R_1 and R_2 are the principal radii of curvature at an arbitrary point on the meniscus of the bridge; R_1 is measured in the xz plane and R_2 is orthogonal to the xz plane. Both R_1 and R_2 can vary along the meniscus. This illustrative example shows the meniscus meeting the solid surfaces at a contact angle of $0°$, which may not be the case for all systems.

For a small static bridge, assuming that internal fluid pressure is spatially constant allows calculation of bridge shape through a force balance approach. Results show that bridge geometry will depend on shape of the bounding solid surfaces, fluid volume, and the contact angle (e.g., Orr et al., 1975; Butt and Kappl, 2009). Increasing the internal fluid pressure towards zero (i.e., atmospheric pressure) would act to expand the bridge and increase the absolute values of both R_1 and R_2 such that the mean curvature approaches zero. As bridge size and internal pressure increase, gravity may act to distort and possibly destabilize the bridge (e.g., Saez and Carbonell, 1990; Kramer, 1998).

Unsaturated flow in coarse granular media occurs along networks of hydraulically connected clasts. Where present, pendular bridges facilitate hydraulic connection for flow both through the interior of porous clasts (e.g., Hu et al., 2004; Carminati et al., 2008; Youngs, 2008) and on the clast surfaces (e.g., Kohonen et al., 2004; Tokunaga, 2009). Given that pendular water will offer little resistance to flow, the geometry of a bridge (size, shape, location) is expected to place an important control on its hydraulic behavior. Therefore, small changes in bridge geometry may alter the macroscopic flow structure. Pendular bridges may also be important elements for liquid storage in granular media. Liquid holdup in packed beds of coarse particles has been observed to increase with fluid flux (e.g., Xiao et al., 2000; Ilankoon and Neethling, 2012). The mechanism for increased storage remains an open question, but can likely be attributed to some combination of bridge volume, film thickness, and/or the number of liquid rivulets on the particle surfaces. Given their potential importance with respect to flow and storage, understanding bridge geometry under flowing conditions is an important prerequisite for prediction of unsaturated flow in coarse granular media.

Here, we present experiments designed to elucidate the hydraulic behavior of pendular bridges under conditions where steady flow is restricted to thin films or rivulets on the clast surfaces. For this situation, flow is driven by gravity and continuity requires that total potential in each bridge must be intermediate to that in the surface films on either side (i.e., upstream > bridge > downstream). Local geometry of the bridge will be controlled by fluid pressure, with the constraint that total potential must smoothly decrease along the flow path. The local fluid pressure is expected to be a complex function of clast geometry, fluid thickness, and flow velocity. Unlike the case of static bridges, fluid pressure in a flowing bridge cannot be predicted solely from clast geometry and contact angle. Instead, we present a simplistic experimental

system designed to closely control flow into a pendular bridge so that we can study its behavior as a function of the flow rate and inclination of the bridge with respect to gravity.

3.3 Experimental Design

The basis of our experimental design was to stack two thin disks in the vertical plane, and then apply water to the upper disk, allowing it to flow along the disk edges under gravity (Figure 3.2). We then measured the pendular bridge that formed on one side of the contact point between the disks as a function of supply rate (Q) and inclination (α) of the paired disks with respect to gravity. The use of disks forces water that flows into the bridge to follow a single, well-defined pathway, and thus isolates the bridge from the spatially and temporally variable flow that would be expected on the surfaces of uniform spheres (Takagi and Huppert, 2010). In addition, establishing a two-dimensional flow system facilitates optical measurement of bridge geometry.

Both of the glass disks used for these experiments had a radius (R_d) of 13.6 mm, and thickness of 0.9 mm. The edges of the disks were ground square to the faces, producing a highly hydrophilic micro-rough surface. The sharp 90˚ angle at the disk edges pins the water film, and inhibits it from advancing onto the disk faces. The disks were placed in point contact and partially bonded to a ~25 x 60 x 1.6 mm sheet of rigid acrylic to assure uniform alignment between trials (Figure 3.2). The side of the contact point nearest to the acrylic sheet was sealed with silicone to constrain the pendular bridge to the opposite side of the contact. The acrylic sheet was then clamped onto a fixture that allowed controlled rotation of the assembly in the xz plane.

Experiments were conducted with the longitudinal axis of the paired disks (z' axis in Figure 3.2) rotated from vertical (z axis) by angles of $\alpha = 0º$, 10º, 20º, 30º and 40º. At each value

of α, independent trials were conducted at supply rates (Q) that varied between 9 and 93

mm^3/min. This range of α and Q was chosen to: (i) maintain a continuous water film that is

restricted to the disk edges, and (ii) produce capillary held pendular bridges between the disks

(i.e., stable with respect to gravity). Prior to each trial, the disk edges were wetted using a

syringe, and the resulting small pendular bridge was evacuated using filter paper. A calibrated

syringe pump was then used to apply deionized water that contained 0.5 ml/l blue food coloring

to the edge of the upper disk from a 20-gauge needle that connected through a ~1 mm thick

column of capillary-held water. Water exited the system by dripping freely from the bottom of

the lower disk.

Image data were collected at a rate of 30 frames per second using two close focus digital

cameras located on opposite sides of the xz plane (Figure 3.2). One camera (Olympus E-PL5

with a 60 mm, f/2.8 macro lens) focused on the pendular bridge (~7 x 4 mm area with 1920 x

1080 pixels; ~3.5 μm/pixel) and the other (Canon Rebel T3 with a 18-55 mm lens) recorded the

entire flow path from the fluid application point to the drip point (~130 x 70 mm area with 1280

x 720 pixels; ~100 μm/pixel). Fiducial marks scribed onto the disk surfaces were used for image

calibration. Boundaries between the disks, water, and the surrounding air were delineated on

individual images using edge detection tools in the MATLAB® software package. Processed

images were used to measure: (i) the cross-sectional area (A) of the pendular bridge in the xz

plane; (ii) radius of curvature of the meniscus at the intersection with the x' axis (R_1 in Figure

3.2); and (iii) thickness of the water film on the disk edges (T_f) away from the bridge.

Uncertainty in delineating the exact contact point between the two disks on the high-resolution

images precluded accurate measurement bridge width ($W_{x'}$ in Figure 3.2).
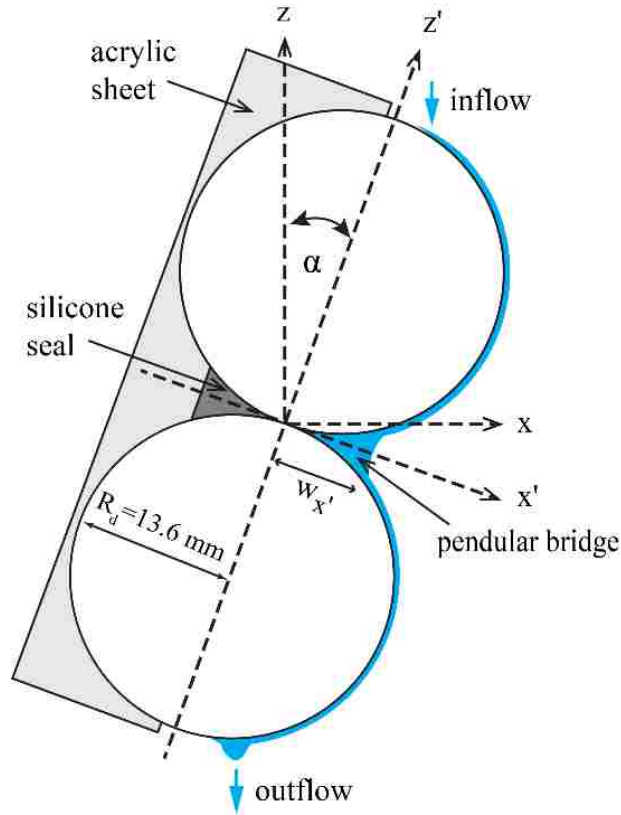
Figure 3.2: Schematic illustration of the experimental apparatus. A portion of each disk ($R_d =$ 13.6 mm) is bonded to a ~25 x 60 x 1.6 mm acrylic sheet that is held in the vertical (xz) plane for all experiments. Flow is restricted to pre-wetted edges of the disks (shaded in blue). The effects of gravity are considered by rotating the longitudinal axis of the disks (z') by an angle of α within the xz plane.

3.4 Results

Flow on the disk edges and through the pendular bridge was continuous from the application site to the drip point at each supply rate (Q) and inclination (α) that was considered. Away from the pendular bridge, water films on the disk edges displayed a convex surface (R_2 in Figure 3.1) that was pinned to the outside corners of the disk edges (no spillover onto the faces). For these edge films, R_1 (Figure 3.1) approximates the disk radius and is of the same sign as R_2 (both are positive). The film begins to thicken (i.e., T_f increases) as it approaches the bridge from either upstream or downstream. Continuing towards the center of the bridge, the meniscus

30

flattens in the xz plane such that curvature ($1/R_1$) first goes to zero, and then reverses sign. The

maximum negative curvature in the xz plane occurs where the bridge intersects the x' axis

(Figure 3.2). The smooth transition from edge film to bridge makes it difficult to distinguish

between these features. We arbitrarily chose to define the bridge as the region about the x' axis

where fluid thickness in the xz plane continuously exceeded the mean film thickness measured

away from the bridge plus one standard deviation ($T_{ave} + \sigma_T$). This definition of the bridge was

visually consistent with the location where $1/R_1 \rightarrow 0$.
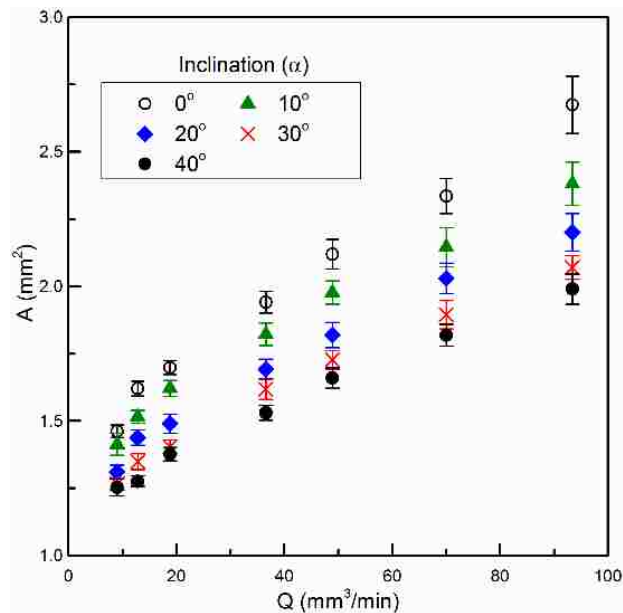
Figure 3.3: Mean cross-sectional area of the pendular bridge in the xz plane (A) is shown as a
function of flow rate (Q) for five values of inclination from vertical (α). Each value represents an
average taken from 60+ images obtained over a 5+ minute interval. The error bars represent one
standard deviation from the mean.

At each value of Q and α, bridge geometry was measured on at least 60 images spaced at

5s intervals (i.e., over a span of 5+ minutes). The mean cross-sectional area of the bridge in the

xz plane (A) was observed to vary with both Q and α (Figure 3.3). At each value of α, A

increased rapidly at the smallest values of Q that were considered, and then at a lesser rate for

larger values of Q. Conversely, bridge area decreased with increasing α at all values of Q. The influence of α increased with Q, as the separation between mean values of A at $\alpha = 0^{\circ}$ and $\alpha = 40^{\circ}$ more than tripled over the 10-fold increase in Q. Differences in A between the tested values of both Q and α were statistically significant (paired-difference test at a significance level of 0.01). The standard deviation of A was small (<0.4A for all trials) and showed a positive relationship with Q, but little dependence on α. Estimated bridge width ($W_{x'}$) remained between ~2.4 and 3.4 mm (i.e., $0.17 < W_x/R_d < 0.25$), which is well below the size where a static bridge would be expected to undergo gravitational drainage (e.g., Saez and Carbonell, 1987). Replicate experiments demonstrated that properties of the bridge were independent of system flow history (no observed hysteresis with respect to Q or α). For a small set of experiments, the flow system was perturbed with volumetric pulses. In each case, the bridge expanded slightly when contacted by the pulse and then shrank back to its original size following passage, thus confirming a lack of hysteresis.

The maximum radius of curvature in the xz plane (R_1) measured where the bridge intersects the x' axis was observed to increase monotonically with Q at each value of α (Figure 3.4). At low values of Q, R_1 for inclinations plotted within a narrow range. As Q increased, the data for R_1 gradually separated and showed an inverse relationship with α at each value of Q. For all trials, a parabola fit to the central part of the meniscus in the xz plane yielded < 3% error in estimating A (Figure 3.5). Differences between the fitted parabola and observed meniscus were not identical about the x' axis. Residuals showed a slight asymmetry of the meniscus about the x' axis, which increased with bridge size. However, the asymmetry was not sufficiently strong to show a statistically significant difference between cross-sectional areas of upper and lower halves of the bridge for any of the trials. In separate experiments, we considered isolated bridges

(no edge films) of similar size to those reported in Figure 3.3. In each case, the meniscus closely followed the arc of a circle over its full length (R_1 = constant). Although our experimental design did not allow direct measurement of R_2, bridge surfaces in the xz plane were slightly convex outwards (positive R_2) with an estimated radius on the order of 10^4 μm.
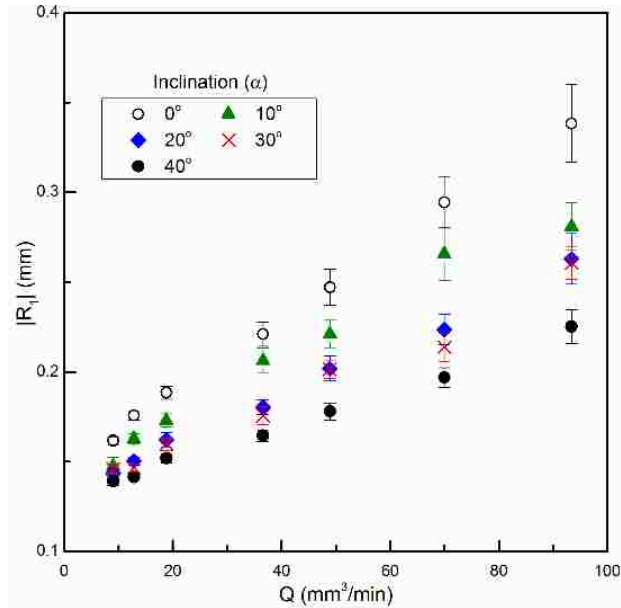
Figure 3.4: Absolute value of the principal radius of curvature in the xz plane (R_1) measured at the center of the meniscus is shown as a function of Q for five values of α. Each value of R_1 is calculated as the focal distance of a parabola fitted to data of the meniscus.

Edge films away from the bridge were not much larger than the pixel size of our imaging system (3.5 μm), thus making uncertainty in the data much higher than for A or R_1. Estimated thickness of the edge films (T_f) increased from 20-37 μm at Q = 9 mm^3/min to 82-105 μm at Q = 93 mm^3/min; there was no clear relationship between T_f and α. Average flow velocity on the disk edge was estimated at the upstream side of the bridge using tracer pulses. Velocity was observed to increase from ~50 mm/s at the smallest supply rate considered, to 90 mm/s at the highest rate. Tracer pulses showed a sharp decrease in velocity across the bridge, and significant mixing.

Flow velocities in the bridge were sufficiently slow that the flow structure was obscured by

diffusion. However, microscopic bubbles of entrained air (or dust) showed complicated motion

within the bridge. A portion of the bubbles closely tracked the edge of the meniscus and moved

relatively rapidly, while others entered the interior of the bridge, following an apparently random

pattern before exiting. Finally, there was a strong temporal correlation between fluctuations in T_f

and in A (coefficient of correlation > 0.98 for all trials). Ancillary experiments were used to

exclude dripping at the downstream boundary as the source of temporal fluctuations, thus they

likely result from either unsteady film flow (Liu et al., 1995; Dragila and Weisbrod, 2003; Lan et

al., 2010) or micro-pulses in the supply from the syringe pump.
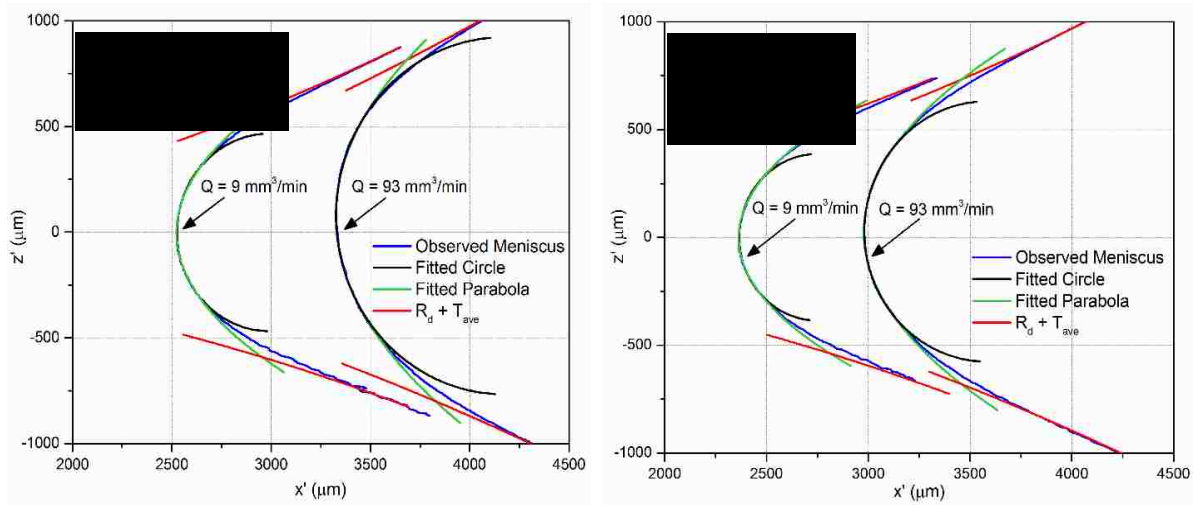
Figure 3.5: Comparison of observed menisci (blue) with fitted parabolas (green) and circles (black) at the lowest and highest flow rates for α = 0° (a) and α = 40° (b). Red lines show the extrapolated outer boundary of water films on disks (R_d+T_{ave}). The separation between the two red lines on upstream or downstream side of the bridge shows the change of film thickness between the two flow rates. The origin of the coordinate system is located at the contact point.

3.5 Discussion

The measured increase in bridge area (A) with Q (Figure 3.3) is attributed to increases in both fluid pressure within the bridge, and film thickness on the disk edges (T_f). A lower bound on bridge width can be estimated from geometric considerations. Given that the disks in our experiment are in point-contact (Figure 3.2), a film flowing on the edge of either disk will intersect the x'' axis at a distance of L from the contact point, where:

$$L = \sqrt{T_f^2 + 2T_fR_d} \qquad \text{Eq. (3.2)}$$

Our experimental data show that the width of the pendular bridge ($W_{x'}$ in Figure 3.2) was always larger than L. The simple model of Eq. (3.2) is flawed because surface tension prevents air-water systems from forming an acute angle where the films meet. However, the functional form of Eq. (3.2) is consistent with our measured data (Figure 3.2); i.e., L increases rapidly at small values of T_f and then at a decreasing rate as T_f increases. Confirming fluid pressure increase within the flow system, mean curvature of films on disk edges increased with Q. Ancillary experiments showed that $1/R_2$ of films increased from ~0.7 mm^{-1} to ~1.1 mm^{-1} between the lowest and highest Q we considered, while R_1 remained constant (defined by radius of the disks). Both R_1 and R_2 of the bridge should increase to accommodate increased fluid pressure within the bridge, leading to an increase of bridge size. The strong functional relationship between A and R_1 suggests that the two parameters are closely linked (Figure 3.6). Since increases of both fluid pressure and T_f with Q favorably act to increase the bridge size, the final geometry of the bridge will be a combination of both factors. The highest Bond number for the bridge is ~1.7 and it implies very small effects of gravity on the bridge geometry (Saez and Carbonell, 1990; Kramer, 1998). However, the weak asymmetry of bridges about the x' axis at

high Q and small α indicates that the effects of gravity becomes noticeable on relatively large bridges.
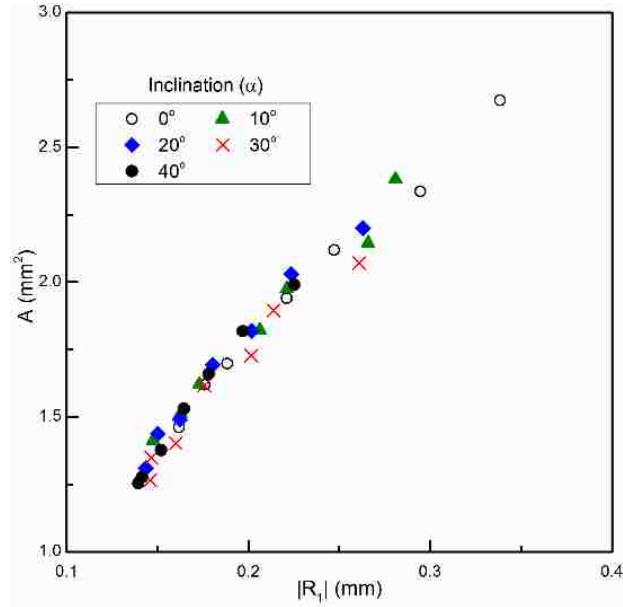
Figure 3.6: Bridge area is shown as a function of the absolute value of R_1 at all inclinations that were considered in our experiments.

The inverse relationship between bridge area (A) and inclination (α) shown in Figure 3.3 is likely due to changes in the slope of the disk edges in the vicinity of the contact. If we hypothesize the bridge geometry to be symmetrical around the x' axis, then flow into the upper-half of the bridge requires the same potential gradient as for flow exiting the lower half of the bridge. The slope of the disc edges is symmetrical around the x' axis at α = 0°, but it becomes asymmetrical when α > 0°, with a lesser slope on the upstream side and a greater slope on the downstream side. As a result of this asymmetry, the gravitational component of the total potential gradient is steeper on the downstream side of the bridge. Therefore, for a given flow rate, continuity of flow requires that fluid pressure at the middle of the meniscus becomes more negative as α increases in order to balance the difference in gravitational potential gradient

between the upstream and downstream sides of the bridge. As predicted by Eq. (3.1), reduction

of fluid pressure in the bridge requires a decrease in R_1, thus the meniscus shifts towards the

contact and reduces A. This analysis suggests that bridge size should increase for $\alpha < 0°$ as

increased fluid pressure would be needed to compensate for the decreased gravitational gradient

on the downstream side of the bridge. In a single trial run at $\alpha = -10°$, water in the bridge started

to spill onto the disk faces for $Q > 9$ mm^3/min, which suggests increased fluid pressure in the

bridge. In addition, attempts to conduct experiments at $\alpha > 40^o$ reduced the gravitational gradient

above the bridge sufficiently that a drip point formed and prevented flow from reaching the

bridge.

Our results help elucidate the processes that cause liquid holdup to increase with

volumetric flow through reactor beds operating under unsaturated conditions (e.g., Schubert et

al., 1986; Urrutia et al., 1996; Xiao et al., 2000). The design of our experiment did not allow

accurate measurement of fluid thickness in the R_2 plane; hence, we cannot calculate fluid

volumes for the bridge or films. However, we did observe that the cross-sectional area of the

bridge (A) increased by a factor of ~1.6 (at $\alpha = 40°$) to 1.8 (at $\alpha = 0°$) over a 10-fold increase in

volumetric flow (Q). Measured values of T_f contained considerable uncertainties, but appeared to

increase by a factor of 2-3 over the same range of Q. This observation is consistent with the

factor of 2.15 that is predicted by models for laterally extensive films (e.g., Bemer and Kalis,

1978; Dragila and Weisbrod, 2003) which assume that $T_f \propto Q^{1/3}$. These results suggest that, in

our specific system, the change in liquid holdup in the pendular bridge was of similar magnitude

to that for the edge films. Extrapolating to three-dimensions, pendular bridges connecting

spheres are likely to form catenoidal surfaces that have a large volume relative to rivulets that

flow on the clast surface. Thus, we expect that the potential for bridge storage will be enhanced

over our two-dimensional system. Our data also showed a lack of hysteresis in A with respect to changing flow conditions and in response to pulsed flow. This result is consistent with those from Ilankoon and Neethling (2012) that attributed strong hysteresis of liquid retention to changes in the number of rivulets on clast surfaces with varying flow rate.

Results of our experiments provide insight into the role that pendular bridges play with respect to unsaturated flow in coarse granular media. Flow on the surface of low permeability clasts must either pass through pendular bridges or circumvent them through dripping. In porous clasts high matric potentials can lead to the formation of surface films (Tokunaga and Wan, 2001), flow through pendular bridges are much higher than that through porous connections between clasts in coarse porous granular media (Carminati et al., 2008). Therefore, the hydraulic properties of individual pendular bridges place a primary control on the spatial distribution of unsaturated flow. We observed that the geometry of a pendular bridge remained unchanged when flow conditions were steady, therefore a relatively stable flow distribution can be expected under steady flow conditions (e.g., Tokunaga et al., 2005). However, any spontaneous change in flow that occurs locally can immediately alter the size of one or multiple bridges in the locality. Change of fluid pressure in those bridges can rapidly transmit along inter-connected flow paths altering properties of numerous bridges and surface films in the flow system producing temporally variable flow distributions in macro-scale flow systems as reported in Jayakody et al. (2011).

Although our experimental set up did not allow direct measurement of R_2 of the bridge, visual observations showed that the absolute value of curvature of the bridge in the xz plane (i.e., $1/|R_1|$) much larger than that orthogonal to the xz plane (i.e., $1/|R_2|$). Setting R_2 of the bridge equals to one-half of the disk thickness (i.e., R_2 at when pressure is close to its maximum) is a

reasonable first-order approximation to evaluate fluid pressure in the bridge. We then used this value of R_2 and measured values of R_1 with Eq. (3.1) to calculate pressure in static bridges formed between two disks and between two spheres. Results of this analysis show that fluid pressure in a bridge formed between two disks is only slightly (~50 Pa) lower than that in a bridge of the same width ($W_{x'}$) formed between two spheres. Therefore, our findings based on this specific flow system are applicable to evaluate the geometry of pendular bridges formed around a point contact between two clasts. Active internal flow observed throughout the bridge indicates the presence of a very complicated flow field within a pendular bridge that is 360° continuous around a point contact. A bridge like this is composed of a set of narrow segments similar to the bridge we tested. Since the effect of gravity on each segment will vary with its orientation, multi-directional flow within the bridge is possible. Furthermore, spatial unevenness of surface flow that enters and exits the bridge will further complicate the hydraulic behavior of the bridge.

3.6 Conclusions

We experimentally investigated the geometry of a pendular bridge under flow-through conditions for several different flow rates and inclinations with respect the gravity. The transition between the bridge and the rivulets above and below was gradual, requiring that we arbitrarily define upstream and downstream boundaries for the bridge. Data show that the size of the pendular bridge increases with the flow rate through it and decreases when the inclination of the bridge with respect to gravity increases. Under flow-through conditions, the cross-sectional profile of the bridge closely resembles a parabola in all cases. In the same system, the profile of static bridges (no internal flow) forms the arc of a circle. Bridge geometry was found to be

independent of flow history of the system, and rapidly adjusts to changing flow conditions. These results can be used to better understand liquid retention and spatial flow structure in unsaturated coarse granular media. Further research on this topic is required to characterize the geometry and internal flow of a three-dimensional pendular bridge. Effects of spatially uneven surface flow and potential gradient within the bridge on bridge geometry and the internal flow field should be thoroughly studied to improve our knowledge of hydraulic behavior of flow-through pendular bridges.

CHAPTER FOUR

IMBIBITION ACROSS A MATRIX-TO-MATRIX CONTACT IN A FRACTURE: A LABORATORY

INVESTIGATION ON EFFECTS OF FRACTIONAL CROSS-SECTIONAL AREA AND POSITION

OF THE CONTACT

4.1 Abstract

Under unsaturated conditions, air-filled fractures can act as barriers to water flow
between adjoining matrix blocks. Matrix-to- matrix contact points and/or liquid bridges formed
due to spatial heterogeneity within a fracture aperture create local hydraulic contacts to facilitate
inter-block flow. Bench-scale experiments were conducted to explore the influence of a matrix-
to-matrix contact on capillary-driven, two-dimensional flow into an initially dry block (9.8 x 1.7
x 6.2 cm) from a saturated block across the contact. We considered: (i) the cross-sectional area of
the contact relative to that of the dry block (A_r), and (ii) the position of the contact relative to
edges of the dry block. Upward imbibition was measured as a function of time for 240 hours
under isothermal conditions. The fraction of the 9.8 x 1.7 cm face in hydraulic contact with the
adjacent saturated block was varied between 0.20 and 1.00. The location of the contact was
varied for each value of A_r.

The rate of imbibition into the dry block varied with both A_r and the location of the
contact. At $A_r = 1.00$, measured imbibition was comparable to one-dimensional absorption-based
predictions, but deviated substantially as A_r decreased. The rate of imbibition was not linearly
dependent on A_r, and at a constant A_r, imbibition rate decreased as the contact shifted closer to
an edge of the block. For all values of A_r, and positions of the contact, imbibition rate decreased
rapidly decreased when the wetting front reached the edges of the block. Saturation (S) of the

41

block at this stage (0.48 ± 0.02) was insensitive to A_r or location of the contact. At the end of 240-hour duration of each trial, S increased to 0.65 ± 0.02 independent of A_r, or location of the contact. These results can be used to better understand matrix-to-matrix flow in unsaturated fractured rock, where air-filled fractures inhibit flow between adjacent blocks.

4.2 Introduction

Despite extensive study over the past several decades, fluid flow and solute transport in unsaturated fractured rock remains a difficult problem that is far from fully understood (e.g. Berkowitz, 2002; Neuman, 2005; Tsang et al., 2015). At the most basic level, a fractured rock contains two flow systems (i.e., fracture network and surrounding porous matrix) that span the same physical space, but have vastly different hydraulic properties. Therefore, not only is it critical to understand the processes that control unsaturated flow within each of these domains, but also the interactions between the two domains. Most research on interaction between these two domains has focused on buffering of fracture flow by the surrounding matrix; i.e., imbibition into an unsaturated matrix during transient fracture flow (e.g., Nitao and Buscheck, 1991; Tidwell et al., 1995; Fairley, 2010). Conversely, much less attention has been paid to explore the effects of fractures on flow through the matrix domain (e.g., Seol et al., 2003).

At sub-zero matric potentials, open (air-filled) fracture apertures act as capillary barriers that prevent flow across the fracture (e.g., Glass et al., 2002). As a result, inter-block flow requires the presence of hydraulic contacts that form local conduits across the fracture. As shown in Figure 4.1, hydraulic contacts may consist of asperity contacts, fracture infilling, or locally accumulated water within the fracture (e.g., Peters and Klavetter, 1988; Glass et al., 1995; Tokunaga and Wan, 1997). For a given fracture, the geometry, location, and number of

inter-block contacts are unknown. Therefore, in continuum-based models it is a common

practice to estimate the fractional area of the fracture planes that is occupied by hydraulic

contacts (A_r, L^2/L^2) and then use that estimate to modify the inter-block conductivity. In effect,

this approach treats the assemblage of contacts as a single large conduit (e.g., Seol et al., 2003),

and thus ignores tortuosity induced by spatially distributed contacts (Glass et al., 1995).

Although A_r can be estimated for macro-scale systems through model calibration (e.g.,

Finsterle, 2000), direct incorporation of inter-block contacts into numerical and conceptual

models requires that we better understand how they influence flow between adjoining matrix
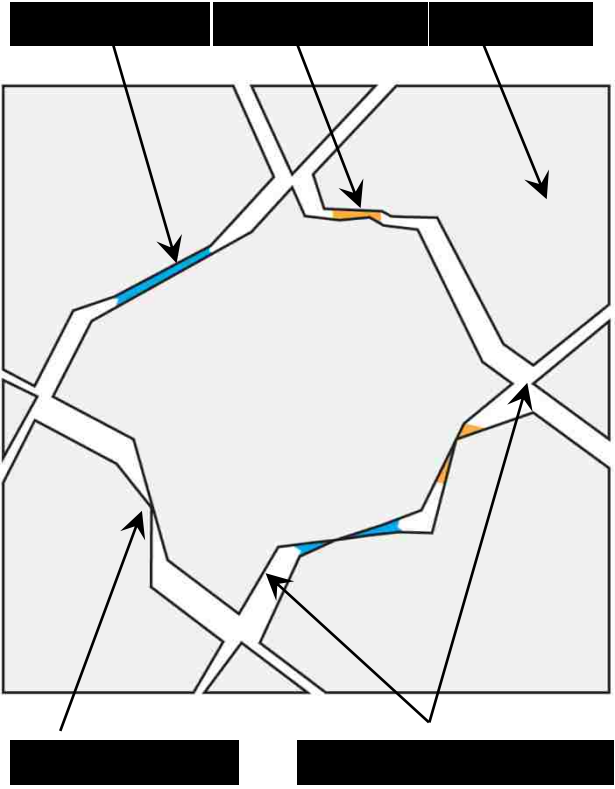
blocks.

Figure 4.1: Conceptual diagram showing hydraulic contacts between fracture blocks at a low matric potential, where most fractures have drained. Air gaps between the fracture walls form local capillary barriers to inter-block flow (i.e., matrix-to-matrix flow). As a result, all inter-block flow must pass through physical contacts that span the fracture, such as asperity contacts, fracture infilling, and/or water accumulated at aperture minima.

In this study, we present experiments designed to evaluate the degree to which hydraulic contacts control capillary-driven imbibition across a fracture. In a series of bench-scale experiments, we measured upward imbibition from a fully saturated block into an initially dry block as a function of time. Upward imbibition was chosen to promote a spatially uniform hydraulic contact across the artificial fracture and stabilize the wetting front with respect to gravity. Imbibition from a saturated block to a dry block was selected to maximize the influence of capillary forces, and reduce environmental effects on the experiment (evaporation, thermal change) by minimizing experimental duration. The fracture blocks were elongated in the vertical direction to force a two-dimensional flow field that allowed direct observation of wetting front advancement in some experiments. In this first set of experiments, we chose to work with a single hydraulic contact, varying both the size of the contact and its location.

4.3 Experimental Design

Upwards imbibition into a dry matrix block (9.8 x 1.7 x 6.2 cm) from an underlying saturated block (10.2 x 2.2 x 1.5 cm) was measured gravimetrically as a function of the hydraulic contact between the blocks (Figure 4.2). The lower block was coated with epoxy on four sides (vertical faces in Figure 4.2), and then cemented into a tank with one of the unsealed 10.2 x 2.2 cm faces protruding by ~1 cm. Hydraulic head in the tank was controlled by an attached water reservoir in which the water level was set to coincide with the base of the upper block. The large surface area (20 x 20 cm) of the reservoir limited the drop in water level during an experiment to < 0.03 cm. The experiment and supply reservoir were each placed on separate electronic balances (0.01 g resolution) to track imbibition into the upper block as a function of time. The

experiment, reservoir, and balances were housed within an enclosure designed to maintain a

constant temperature (23.5 ± 0.5 °C) and to minimize air currents.
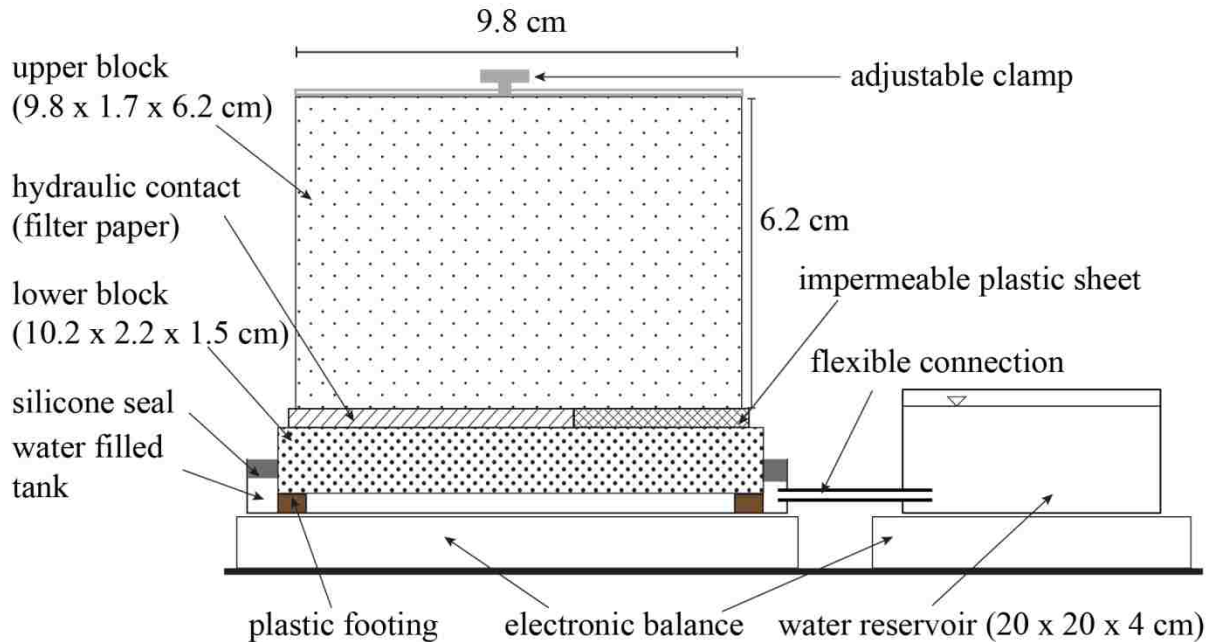
Figure 4.2: Schematic illustration of the experimental apparatus (not drawn to scale) configured for an end contact. The external framework holding the blocks in place is not shown. The water-filled tank contains only a small volume of water and was designed to be sealed against tension. The flexible connection to the water reservoir prevents mass changes in one part of the system from affecting the other. Hydraulic head in the reservoir is set to be approximately level with the base of the upper block (near zero head under static conditions). A design goal for this apparatus was to minimize total mass so that water uptake by the upper block is clearly discernible.

A single set of test blocks (upper and lower) were cut from a sample of Aztec Sandstone

(Hewett, 1931), and thoroughly leached with deionized water prior to use. This silica-cemented

sandstone was chosen for its relatively uniform hydraulic properties and capacity to imbibe

easily measurable quantities of water over a period of hours to days (i.e., imbibition >>

evaporative loss). This material is also mechanically stable, chemically inert, and has a light

color that facilitates visual observation of wetting front advancement. The average pore diameter

(~20 μm) estimated through optical petrography suggests that capillary rise under dry conditions

would be on the order of 1.47 m at 25 °C. The upper block holds 13.5 ± 0.1 g of water at full

saturation (S = 1.00), which gives an effective porosity of n = 0.13. Saturated hydraulic

conductivity ($K_{sat} = 3 \times 10^{-3}$ cm/hour at 25 °C) was obtained from a falling head test. Filter paper

was used to control hydraulic communication between the blocks (thickness ~0.15 cm, $K_{sat} = 70$

cm/hour, n depends on compression). The high conductivity and deformability of the filter paper

assured that hydraulic properties of the contact have a negligible effect on observed behavior;

i.e., cross-sectional area of the contact controls behavior.

Prior to each trial, the upper block was dried for 24 hours at 105 °C, and then sealed on

five sides with plastic heat-shrink wrap to minimize evaporative loss. A pinhole at the top

allowed air to escape during imbibition. Next, the tank holding the lower block was vacuum

saturated and connected to the water reservoir. Experiments were initiated by clamping the

unsealed 9.8 x 1.7 cm face of the dry upper block on top of the lower block with a strip of filter

paper sandwiched in between. The top of the lower block was intentionally cut to be larger than

the matching face on the upper block so that imbibition would not be sensitive to alignment of

the blocks. A rubber membrane surrounding the contact was employed to minimize evaporative

loss. Data from the balances and environmental sensors (temperature, humidity, barometric

pressure) were collected at 2-minute intervals throughout the course of each trial (> 240 hours).

Independent measurements of mass change in the upper block before and after each trial

validated the experimental data on water uptake to within 2%.

The cross-sectional area of the contact between the two blocks was varied between trials

by changing the length of the filter paper, while keeping the width constant at 2.0 cm. In the

baseline experiment ($A_r = 1.00$), the interface was completely covered with filter paper. At A_r

<1.00, a portion of the filter paper was replaced with impermeable plastic sheet to provide

mechanical support and prevent vapor-phase transfer into the upper block. Trials were conducted ($A_r < 1.00$) with the filter paper placed: (i) at the center of the block (center contact); and (ii) against one end of the block as shown in Figure 4.2 (end contact). To consider the influence of the lower block, one trial was run in which the upper block was placed in a ~1 mm deep layer of water, then removed and weighed at regular intervals over a 24 hour period (referred to as the free-water trial). In addition, a small number of short duration (< 48 hours) experiments were performed outside of the environmental enclosure so that we could visually observe wetting front advancement.

4.4 Results

Quantitative experiments performed inside the environmental enclosure showed that saturation (S) of the upper block increased monotonically in all trials (Figure 4.3). The rate of imbibition (dS/dt) was most rapid for the free-water trial (no lower block). For imbibition from the lower block (main experiments), dS/dt declined both with decreasing A_r and when the contact was moved from the center of the block to one end. Despite the clear differences in dS/dt between the trials (Figure 4.3), saturation of the upper block at $t = 240$ hrs was 0.65 ± 0.02 independent of A_r, or location of the contact (note that Figure 4.3 ends at $t = 72$ hrs to better elucidate early-time behavior). The data shown in Figure 4.3 suggests that dS/dt passed through three distinct stages of behavior. The rate of imbibition is most rapid at the start of each trial ($t = 0$) and then declines gradually to produce a mildly concave curve up to a saturation of about 0.50 (Stage 1). After that, the imbibition rate declines rapidly over a range of saturation that extends from roughly 0.50 to 0.58 (Stage 2). Finally, in Stage 3, dS/dt shows little change through the end of the experiment, remaining at ~ 0.007 ± 0.002/day for all trials.
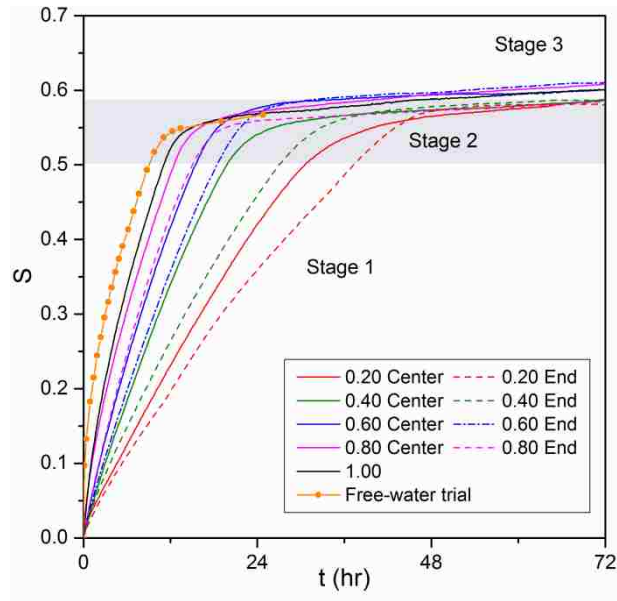
Figure 4.3: Saturation (S) of the upper block is shown as a function of time (t), contact area (A_r), and location of the contact. Trials with a center contact are shown as solid lines, while the dash lines show trials with an end contact. The line with round markers represents data from the free-water trial that ran for 24 hours. For trials running the full 240 hours, the imbibition rate (dS/dt) remained essentially constant for $t \geq 72$ hours (not shown). Saturation at 240 hours was 0.65 ± 0.02 independent of A_r or location of the contact.

One-dimensional imbibition under capillary dominated conditions (horizontal, zero head at inlet) has been shown to scale linearly with the square root of time (e.g., Philip, 1957a). In our experiments, the static (pre-imbibition) hydraulic head at the bottom of the upper block was near zero and gravitational effects were expected to be small with respect to capillarity; thus, we analyzed our early time data by plotting S as a function of $t^{0.5}$ (Figure 4.4). We arbitrarily defined the end of Stage 1 to occur where the slope of S vs. $t^{0.5}$ started to continuously decrease. Stage 1 data for the free water experiment is clearly linear over most of the range; the initial shift to the left is believed to be an experimental artifact (Figure 4.4).

48
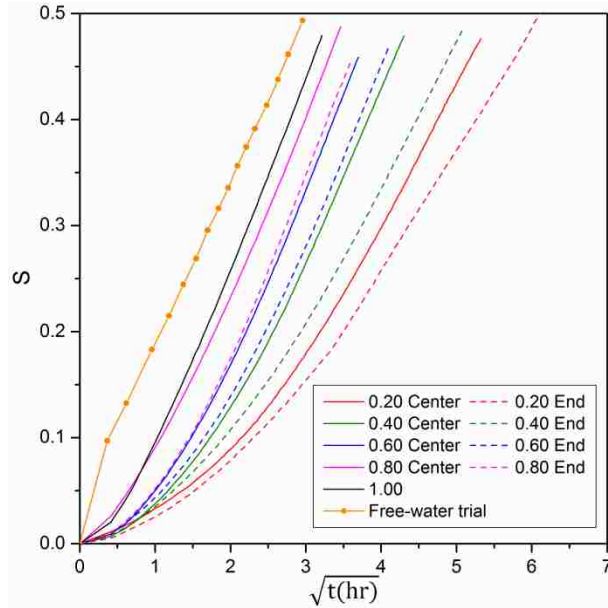
Figure 4.4: Saturation (S) of the upper block during Stage 1 imbibition is shown as a function of the square root of time ($t^{0.5}$), contact area (A_r), and location of the contact. Trials with a center contact are shown as solid lines, while the dash lines show trials with an end contact. The single line with round markers represents data from the free-water trial. The end of Stage 1 was taken to be the time when the slope of S vs. $t^{0.5}$ began to undergo continual decline; therefore, the final S at the end of Stage 1 differs between trials.

In all other experiments, the data is concave upwards near t = 0, and then gradually transforms into a straight line throughout the remainder of Stage 1. For A_r = 1.00, the transformation occurred at t = 0.5 hr and S = 0.05. As A_r decreases, the linear portion of the data begins at later times, but at S ~ 0.15 - 0.18 for all contacts. In addition, the slope of the linear portion decreases with decreasing A_r. At constant values of A_r, experiments with a center contact showed an earlier transition to linear behavior than those with an end contact. The slope of the linear portion was also steeper for a center contact than for an end contact. In all trials, S at the end of Stage 1 was 0.48 ± 0.02 regardless of A_r or the position of the hydraulic contact. Conversely, the time at which Stage 1 ended was highly dependent on both A_r and the position of the contact (Figure 4.5).

49
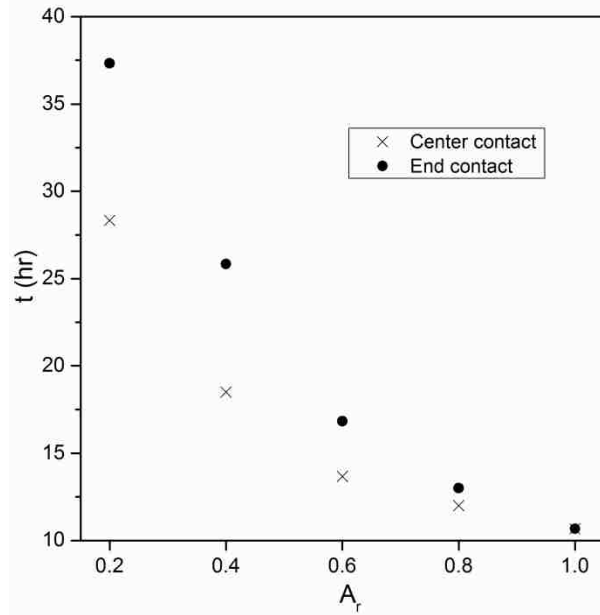
Figure 4.5: Time (t) at which Stage 1 ended as a function of A_r and the position of the contact. At the end of Stage 1, saturation of the upper block reached to 0.48 ± 0.02 independent of A_r or the position of the contact.

Experiments conducted outside of the environmental enclosure allowed direct observation of wetting front dynamics (Figure 4.6), but limited our ability to collect quantitative data. In all trials, the visually defined wetting front formed a smooth line that showed small bumps indicative of local heterogeneity, but no sharp breaks. Visual sharpness of the wetting front appeared to decrease with both time and A_r. We also noted that advancement of the wetting front slowed substantially as it approached the block boundaries. This slowing coincided with the end of Stage 1 behavior. The influence of the hydraulic contact can be seen clearly in Figure 4.6. At $A_r = 1.00$, the wetting front remained nearly horizontal throughout the experiment. For experiments with a center contact, the front was concave downwards and nearly symmetrical about the vertical axis. The front formed a steep slope where it met the bottom of the upper block (contact). The wetting front curvature increased as A_r decreased. In all trials with a center contact, the wetting front flattened out a bit after contacting the vertical sides of the slab and

50

concavity continued to decrease as it approached the top. For end contacts, the wetting front was approximately horizontal where it contacted the vertical edge above the contact and sloped away from that corner forming a concave downwards shape. At small values of A_r (0.20 and 0.40) with an end contact, the wetting front reached the top of the slab before the opposite vertical edge.
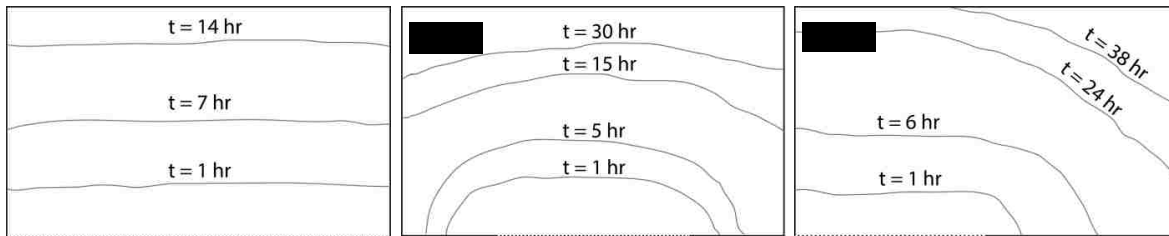
Figure 4.6: Wetting front position on the 9.8 x 6.2 cm face of the upper block, inferred from visual observation of experiments conducted outside the environmental enclosure. Illustrative examples are shown for: (a) A_r = 1.00, (b) center contact with A_r = 0.50, and (c) end contact with A_r = 0.50. The rubber membrane that minimized evaporation from the contact area was not installed in these experiments to allow observation of the entire upper block. The resulting evaporative loss and the effects of temperature fluctuations (internal condensation, evaporation) impacted quantitative data from these experiments. However, the general patterns shown in Figure C remained, allowing us to interpret the mechanisms responsible for the three stages of imbibition.

4.5 Discussion

Measurements of capillary-dominated upward imbibition into an initially dry block of sandstone from a saturated block of the same rock show a strong dependence on the fractional cross-sectional area of the contact and the location of the contact. Non-linearity at the start of each experiment is attributed to restriction of flow entering the upper block. Material used to form hydraulic connections between the blocks exhibits conductivity that exceeds that of the lower block by > 4 orders of magnitude (K_{sat} of filter paper >> K_{sat} of blocks), thus we attribute flow restriction to energy loss in the saturated lower block (e.g. Peters and Klavetter, 1988).

Compared to direct imbibition from a pool of water (fracture-filled water or surface films), supply through a wet block leads to loss of energy in water before reaching the dry block significantly reducing the imbibition rate. Considering the average rate of the first two hours of the flow in our experiment, hydraulic head loss for $A_r = 1.00$ is estimated to be ~ 27 cm, which makes the hydraulic head at the bottom of the upper block approximately -25.5 cm. This decrease, compared to zero pressure in free-water trial, reduces the calculated sorptivity of the upper block (Philip, 1957b) from 0.154 to 0.070 cm/hr$^{\frac{1}{2}}$ when the saturated block is inserted between water pool and upper block.

Flow data show that both fractional cross-sectional area (A_r) and location of the contact with respect to edges of the block place a primary control on imbibition into the block. As briefly presented in the previous section, flow into the upper slab can be separated into three stages (Stage 1, 2 and 3) based on the rate of saturation increase over time. Properties of the contact critically influence flow during Stage 1, which is characterized by very high dS/dt as a result of initially high potential gradient within the upper block. Changes in A_r affect flow by altering transmissivity of the contact and hydraulic head loss in the lower block. Effective transmissivity of the contact is a linear function of only A_r. Therefore, shrinking of the contact reduces its ability to facilitate a large volumetric flow under a given potential gradient. However, data presented in Figure 4.3 show that imbibition rate is not linearly dependent on A_r for any type of contact. Because of the geometry of the wetting front, initial potential gradient within the upper block is much higher for small A_r and it decreases at a slower rate compared to those for large A_r. Therefore, flux through the contact significantly increases with decreasing A_r (Figure 4.7) producing a non-linear relationship between imbibition rate and A_r. In addition to effect of transmissivity, a reduction in A_r lowers the effective flow area of the lower block increasing the

head loss in it. This can lead to a lower hydraulic head at the contact, but data (Figure 4.8) show

that this effect is considerable only for $A_r = 0.20$ because of the geometry of our lower block

(low height/length ratio).
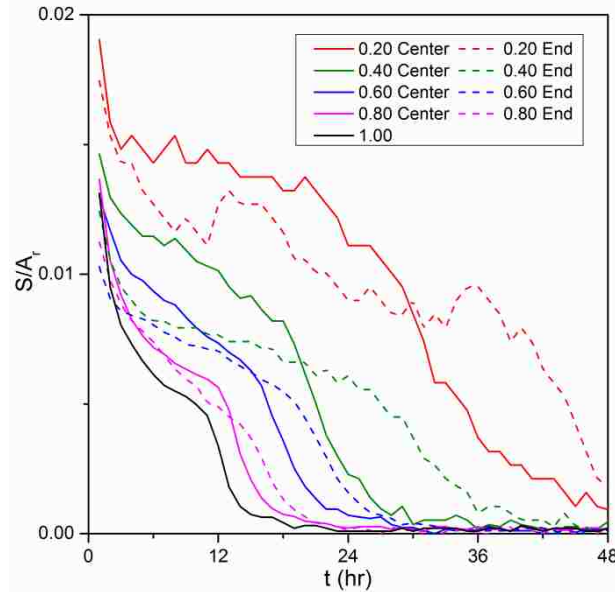
Figure 4.7: Change of flux across the hydraulic contact is shown as a function of time (t), contact area (A_r), and location of the contact. Trials with the center contact are shown with solid lines, while the dash lines show trials with the end contact. Flux is presented in dimensionless form as the saturation per unit cross-sectional area of the contact.

The location of the contact relative to edges of the upper block dictates the development

of flow field, thus significantly controls the imbibition rate. A center contact allows the flow

field to develop laterally in either side of it, until the wetting front reaches two vertical edges of

the block. Moving the contact towards an edge of the block causes the wetting front to contact

the adjacent vertical edge within a short duration, preventing further expansion of the flow field

in that direction. In the end-member scenario, where the contact is located against an edge of the

block, flow field is forced to develop only in one lateral direction (Figure 4.6) significantly

lowering the imbibition rate compared to that of a center contact of similar A_r (Figure 4.3). For

most part of Stage 1 flow at any value of A_r, duration to reach a given saturation (S) with the center contact ($t_{S,Ar,center}$) and at end contact ($t_{S,Ar,end}$) show the following relationship:

$$t_{S,Ar,center} = (0.80 \pm 0.03) \, t_{S,Ar,end} \qquad \text{Eq. (4.1)}$$
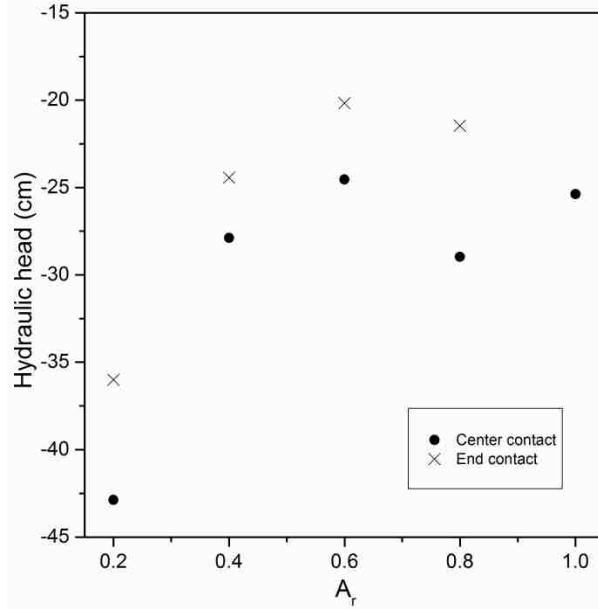
Figure 4.8: Approximated average hydraulic head at the contact during the first two hours of flow as a function of A_r and location of the contact. Hydraulic head was calculated assuming one-dimensional flow through the lower block and using the observed volumetric flow rates. Water in the external reservoir (Figure 4.2) applies a total hydraulic head of ~1.7 cm at the bottom of the lower block.

Characteristics of S vs $t^{0.5}$ plot (Figure 4.4) indicate mechanisms associated with Stage 1 flow. For one-dimensional imbibition, this plot is expected to be linear. However, the plot for A_r = 1.00 becomes linear at t ~ 0.5 hr, which indicates approximate time scale required to develop a stable hydraulic communication between the lower and upper blocks through the contact. Delayed transition of S vs $t^{0.5}$ plot from concave upward to linear form for smaller contacts ($A_r <$ 1.00) implies the presence of other processes that affect the flow. Gradually increasing slope of S vs $t^{0.5}$ graph for these trials shows an increase in "apparent sorptivity" of the upper block (i.e., sorptivity affected by the flow boundary and wetting front) with the evolution of the flow field.

54

The total magnitude of capillary forces on water is proportional to the length of the wetting front. Because of the curved geometry (at $A_r < 1.00$), length of an advancing front gradually increases (Figure 4.6), raising the capillary force on water. This effect causes to gradually increase the slope of S vs $t^{0.5}$ plot. For an end contact, the slope of the plot increases slower than that for the center contact of the same A_r, because of the shorter length of the wetting front compared to the front for the center contact. After the gradual increase, S vs $t^{0.5}$ becomes linear when changes in the wetting front length does not affect flow between the blocks. At this time, sorptivity of the upper block is determined by the potential gradient and transmissivity of the contact.

Stage 2 flow, which is characterized by rapidly decreasing dS/dt, starts when migration of the wetting front stops when it reaches all edges of the block. A saturation gradient exists behind an advancing wetting front (Zimmerman et al., 1990; Tidwell et al., 1995). After the leading edge of the front contact all edges of the block, relatively small pores that exist immediately behind it are filled at a rate comparable to that at the end of Stage 1. Since the volume of unfilled pores that has a low water entry pressures and easily accessible to water is relatively small, this process ends within a short duration. During stage 2, relatively low sorptivity of the upper block limits imbibition, and properties of the hydraulic contact have less effect on flow. However, at A_r = 0.2, change in dS/dt is significantly slower compared to that for larger contacts, which implies that low transmissivity of the contact can considerably restrict the flow. Because of slow pore-filling mechanism during this stage, location of the contact does not noticeably affect flow at any value of A_r. Stage 3 flow, which is characterized by very slow and nearly steady saturation increase results from gradual filling of relatively large pores in the already wet block. This process is very slow because of trapped air in unfilled pores and relatively high water entry

pressure for large pores. Therefore, flow into the block is entirely controlled by its sorptivity independent of the connection.

We attempted to develop an empirical relationship between S, A_r and t for all contacts. Instead of three stages of flow described above, we assumed two stages of flow; early stage and late stage to simplify our approach. The early stage continues until S = 0.53, which is a value selected based on the observed mid-point of Stage 2 for A_r = 1.00. We find that, for our specific flow system, duration of Stage 1 at A_r = 1.00 ($t_{stage1,Ar=1.00}$) and duration to increase the saturation to a given value (S) within Stage 1 with an end contact of any value of A_r show the following relationship:

$$\left(\frac{t_{S,Ar,end}}{t_{stage\,1,Ar=1.00}}\right)^{0.5} = -(1.38S + 0.37)A_r + 3.00S + 0.52 \quad \text{Eq. (4.2)}$$

The rate of saturation increase for the late stage is equal to that was observed during Stage 3 flow at A_r = 1.00. Therefore, using Eq. (4.1), (4.2), and experimentally measured parameters at A_r = 1.00 (i.e., $t_{stage1,A=1.00}$ and dS/dt during Stage 3), we can estimate the time required to reach a specific saturation for any contact. When S > ~0.05 (i.e., after a steady hydraulic communication between the two blocks has established), the maximum difference between estimated and observed saturations for t < 72 hr is ± 0.05 for a given contact (Figure 4.9). The y-intercept of estimated S vs t plot is always negative with the lowest value of -0.16 (for A_r = 0.20), because or estimation is mainly based on the observed data where S vs $t^{0.5}$ is linear. Though these empirical equations (Eq. 4.1 and 4.2) are valid only for our flow system, they show that effects of A_r and location of a hydraulic contact on imbibition can be incorporated into numerical models.
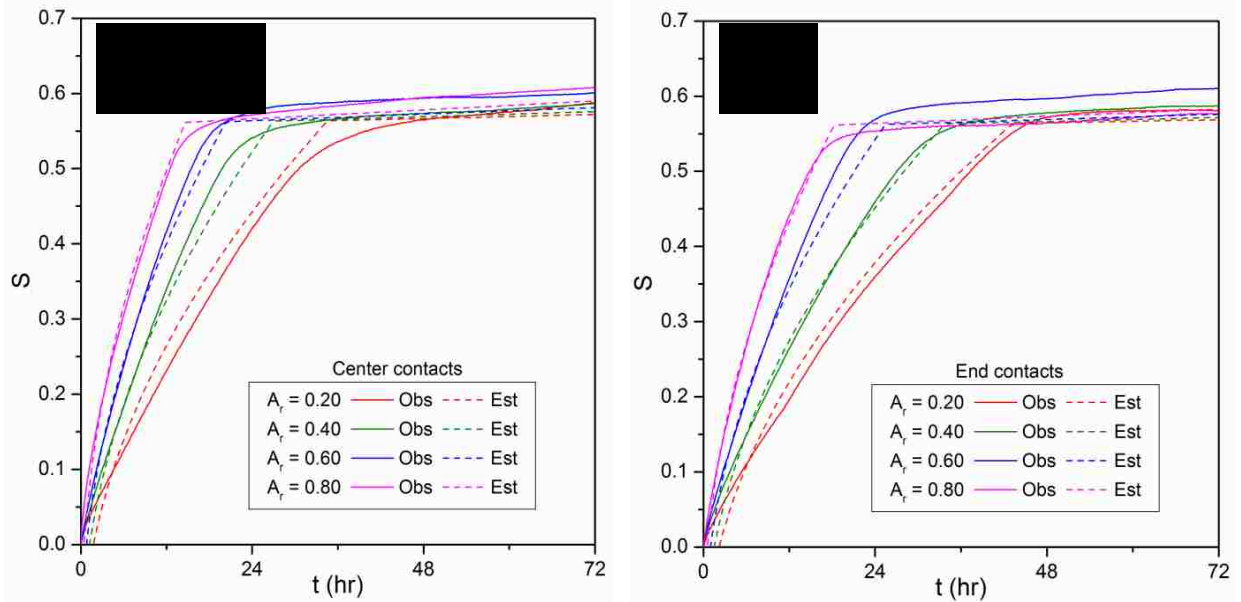
Figure 4.9: Observed and estimated saturations of the upper block are given as a function of time (t), contact area (A$_r$), and location of the contact. Observed values are shown in solid colors, while the dash lines show trials with the end contact. Results for the center and end contacts are presented in (a) and (b), respectively.

4.6 Conclusions

Data show that fractional cross-sectional area of a hydraulic contact and its position with respect to boundaries of the block significantly affect matrix-to-matrix imbibition. The rate of imbibition is not linearly dependent on the cross-sectional of the contact. Shifting the contact toward an edge of the block significantly reduces the imbibition rate. Effects of the above two properties of a contact are mostly for Stage 1 flow, where the wetting front continuously advances in the block. Flow characteristics during stage 2 and 3 are effects of boundaries of the block that impede flow beyond the block. Overall flow characteristics observed in our experiments are expected occur in porous blocks bound by air-filled fractures that inhibit matrix-to-matrix flow (e.g., Glass et al., 2002; Wood et al., 2004) before hydraulic connections to neighboring blocks develop at high matrix saturation. Therefore, incorporating effects of both

57

cross-sectional area and spatial distribution of individual hydraulic contact within a considered

flow domain in fractured media is important to accurately characterize the flow. This will be

critical in predicting the development of macro-scale flow field with infiltration.

CHAPTER FIVE

SUMMARY

This dissertation presents three projects designed to explore the influence of hydraulic connections (also known as hydraulic bridges and hydraulic contacts) on unsaturated flow in dual-permeability media. Large inter-clast pores in coarse granular media drain at near zero matric potentials requiring that hydraulic bridges formed by porous contacts or pendular water facilitate liquid transfer between adjacent clasts. Unsaturated flow in fractured media also experiences this phenomenon, despite contrasting pore geometries in two types of media. Because of these reasons, understanding the behavior of hydraulic contacts is important to accurately predict unsaturated flow and solute transport in dual-permeability media.

Numerical simulations performed to examine how the cross-sectional area and hydraulic conductivity of a bridge influence steady-state flow through a spherical clast are presented in the second chapter of the dissertation. The third chapter presents a series of bench-scale experiments performed to evaluate the geometry of a pendular bridge under various flow-through conditions and at different inclination of the bridge with respect to gravity. The fourth chapter describes bench-scale experiments that were conducted to explore the influence of matrix-to-matrix hydraulic contacts on imbibition into a matrix blocks. We can summarize the major findings of these studies as follows.

At steady state, volumetric flow through a spherical clast (Q) shows a non-linear dependency on the cross-sectional area of hydraulic bridges with respect to that of the clast (A_r). Flow is more sensitive to changes in conductivity of the bridges when it is lower than that of the clast, but A_r places the primary control on flow for other bridges. Flow distribution within the clast expands as A_r increases. Bridges that are more conductive than the clast promote this

behavior, while less conductive bridges retard it. When flow-through condition is present, the size of a pendular bridge increases with the flow rate through it (Q) and decreases with increasing inclination of the bridge from vertical (α). Bridge geometry is independent of flow history of the system and immediately adjusts to changing flow conditions. The meniscus of a bridge formed under flow-through condition closely resembles a parabola while that formed under static conditions resembles the arc of a circle. When matrix-to-matrix imbibition in to a porous block is considered, cross-sectional area of a hydraulic contact relative to that of the block (A_r), and location of the contact relative edges of the block significantly control imbibition. The rate of imbibition non-linearly decreases as A_r decreases. At constant A_r, shifting the contact towards an end of the block reduces the imbibition rate. If the block is hydraulically isolated with the exception of the considered connection, saturation of the block when the wetting front contacts all boundaries of the block will be independent of the contact (0.48 in our experiments).

Unsaturated flow in dual-permeabilty media is influenced by many factors, but saturation-dependent hydraulic conductivities, interaction between two flow domains, varying control of gravity and capillary forces on flow, as well as spatially and temporally variable hydraulic bridges are the dominant factors. Our primary objective in this research was to understand how hydraulic bridges affect flow and liquid holdup. Because of very complex nature of flow in real systems, we used simplified systems to isolate the effects of considered factors in each study. Future studies should incorporate other factors that influence a flow system, thus the conceptual systems can better resemble real flow systems. Below we discuss about potential future research on each study presented in this dissertation.

5.1 Influence of Hydraulic Bridges on Flow in Coarse Porous Clasts

The major simplifications in the numerical model were solely gravity-driven flow, the absence of surface flow on the clast (both assuming satiated saturation of the clast), and spatially uniform hydraulic conductivity of the bridge. Below the satiated saturation, capillary forces will produce diffusive flow within the clast (Carminati et al., 2007). Furthermore, hydraulic conductivity of the clast will vary with matrix saturation. Therefore, flow mechanism will become more complicated than that considered in our simulations. When the saturation increases above the satiated level, liquid films starts to form on clast surfaces (Tokunaga and Wan, 2001). As a result, water can enter or exit the clast matrix through the entire surface creating a very complex intra-clast flow field. Hydraulic conductivity of a bridge that is a combination of a porous contact and pendular water varies between the two components of the bridge. Hydraulic properties of each component will affect volumetric flow through the entire system and spatial flow distribution in the system. These situations should be addressed in future work. Furthermore, advective and diffusive transport of solutes should be incorporated into the model to evaluate dissolution and transport of materials within the clast.

5.2 Geometry of Flow-through Pendular Bridges

We monitored the geometry of a pendular bridge formed between two disks enabling us to maintain a relatively steady flow to the bridge and precisely measure the two-dimensional geometry of the bridge employing optical methods. In a flow system composed of two spherical clasts, fluid supply to the bridge may not be spatially uniform due to unsteady surface flow (Liu et al., 1995; Dragila and Weisbrod, 2003; Lan et al., 2010; Takagi and Huppert, 2010). Furthermore, fluid pressure distribution within a three-dimensional bridge will change in a

complex manner with the inclination of the bridge due to its geometry. Therefore, future research on this topic should explore the geometry and internal flow of a three-dimensional pendular bridge. Stability of a flow-through bridge with respect to gravitational drainage is another important topic that should be explored. Force-balance approach has been successfully used to numerically study the stability of static pendular bridges (e.g., Saez and Carbonell, 1990), but applying this method for flow-through bridges is extremely difficult due to gradual transition between surface films and the bridge, as well as flow within the bridge. Therefore, stability of a three-dimensional pendular bridge should be studies experimentally.

5.3 Imbibition across Matrix-to-matrix Contacts

We studied two-dimensional imbibition into a porous block through well-characterized hydraulic contacts. This simplified flow system allowed us to focus on the influence of the fractional cross-sectional area and location of a contact on imbibition. Future research should investigate how an individual hydraulic contact affects three-dimensional imbibition and how to apply the findings of this research to large-scale flow systems. Numerical modeling of three-dimensional transient flow involves numerous untested assumptions, and heavily relies on model calibration parameters. Validity of these assumptions should be tested in physical experiments and flow mechanisms should be thoroughly understood to improve process-based flow models. Applying findings of bench-scale or meso-scale experiments on real flow systems remains a challenge. Therefore, future work should consider up-scaling or down-scaling parameters and processes in controlled experiments to apply on other systems.

REFERENCES

Badiozamani, K., Mackenzie, F., & Thorstenson, D. (1977). Experimental carbonate cementation; salinity, temperature and vadose-phreatic effects. *Journal of Sedimentary Research, 47*(2), 529-542.

Bartlett, R. W. (1997). Metal extraction from ores by heap leaching. *Metallurgical and Materials Transactions B, 28*(4), 529-545.

Bear, J., Rubinstein, B., & Fel, L. (2011). Capillary pressure curve for liquid menisci in a cubic assembly of spherical particles below irreducible saturation. *Transport in Porous Media, 89*(1), 63-73.

Bear, J. (1988). *Dynamics of fluids in porous media* Dover Publications.

Bemer, G., & Kalis, G. (1978). A new method to predict hold-up and pressure drop in packed columns. *Trans.I.Chem.Eng, 56*, 200.

Berkowitz, B. (2002). Characterizing flow and transport in fractured geological media: A review. *Advances in Water Resources, 25*(8), 861-884.

Berli, M., Carminati, A., Ghezzehei, T. A., & Or, D. (2008). Evolution of unsaturated hydraulic conductivity of aggregated soils due to compressive forces. *Water Resources Research, 44*, W00C09. doi:10.1029/2007WR006501

Butt, H., & Kappl, M. (2009). Normal capillary forces. *Advances in Colloid and Interface Science, 146*(1-2), 48-60. doi:10.1016/j.cis.2008.10.002 ER

Carminati, A., & Fluehler, H. (2009). Water infiltration and redistribution in soil aggregate packings. *Vadose Zone Journal, 8*(1), 150-157. doi:10.2136/vzj2008.0077

Carminati, A., Kaestner, A., Lehmann, P., & Fluhler, H. (2008). Unsaturated water flow across soil aggregate contacts. *Advances in Water Resources, 31*(9), 1221-1232. doi:10.1016/j.advwatres.2008.01.008

Carminati, A., Kaestner, A., Hassanein, R., Ippisch, O., Vontobel, P., & Fluehler, H. (2007). Infiltration through series of soil aggregates: Neutron radiography and modeling. *Advances in Water Resources, 30*(5), 1168-1178. doi:10.1016/j.advwatres.2006.10.006

Carminati, A., Kaestner, A., Ippisch, O., Koliji, A., Lehmann, P., Hassanein, R., . . . Fluehler, H. (2007). Water flow between soil aggregates. *Transport in Porous Media, 68*(2), 219-236. doi:http://dx.doi.org/10.1007/s11242-006-9041-z

Conca, J. L., & Wright, J. (1992). Diffusion and flow in gravel, soil, and whole rock. *Applied Hydrogeology, 1*(1), 5-24.

Dragila, M. I., & Weisbrod, N. (2003). Parameters affecting maximum fluid transport in large aperture fractures. *Advances in Water Resources, 26*(12), 1219-1228. doi:10.1016/j.advwatres.2003.09.002

El Boushi, I. M., & Davis, S. N. (1969). Water-retention characteristics of coarse rock particles. *Journal of Hydrology, 8*(4), 431-441.

Fairley, J. P. (2010). Fracture/matrix interaction in a fracture of finite extent. *Water Resources Research, 46*(8)

Finsterle, S. (2000). Using the continuum approach to model unsaturated flow in fractured rock. *Water Resources Research, 36*(8), 2055-2066.

Ghezzehei, T. A., & Or, D. (2000). Dynamics of soil aggregate coalescence governed by capillary and rheological processes. *Water Resources Research, 36*(2), 367-379. doi:10.1029/1999WR900316

Glass, R. J., Nicholl, M. J., Pringle, S., & Wood, T. (2002). Unsaturated flow through a fracture–matrix network: Dynamic preferential pathways in mesoscale laboratory experiments. *Water Resources Research, 38*(12)

Glass, R. J., Nicholl, M., & Tidwell, V. (1995). Challenging models for flow in unsaturated, fractured rock through exploration of small scale processes. *Geophysical Research Letters, 22*(11), 1457-1460.

Hewett, D. F. (1931). *Geology and ore deposits of the goodsprings quadrangle, nevada* US Gov't. Print. Off.

Hu, Q. H., Kneafsey, T. J., Roberts, J. J., Tomutsa, L., & Wang, J. S. Y. (2004). Characterizing unsaturated diffusion in porous tuff gravel. *Vadose Zone Journal, 3*(4), 1425-1438.

Ilankoon, I., & Neethling, S. (2012). Hysteresis in unsaturated flow in packed beds and heaps. *Minerals Engineering, 35*, 1-8.

Jayakody, J., Nicholl, M., & Simon, A. (2011). Spatial and temporal structure of unsaturated flow in porous crushed stone. Paper presented at the *43rd Symposium on Engineering Geology and Geotechnical Engineering 2011: Water, Soils and Sustainability in the Intermountain West,* 98-106.

Kohonen, M. M., Geromichalos, D., Scheel, M., Schier, C., & Herminghaus, S. (2004). On capillary bridges in wet granular materials. *Physica A: Statistical Mechanics and its Applications, 339*(1), 7-15.

Kramer, G. (1998). Static liquid hold-up and capillary rise in packed beds. *Chemical Engineering Science, 53*(16), 2985-2992.

Lan, H., Wegener, J., Armaly, B. F., & Drallmeier, J. (2010). Developing laminar gravity-driven thin liquid film flow down an inclined plane. *Journal of Fluids Engineering, 132*(8), 081301.

Liu, J., Schneider, J., & Gollub, J. P. (1995). Three-dimensional instabilities of film flows. *Physics of Fluids (1994-Present), 7*(1), 55-67.

Lu, N., Lechman, J., & Miller, K. T. (2008). Experimental verification of capillary force and water retention between uneven-sized spheres. *Journal of Engineering Mechanics-Asce, 134*(5), 385-395. doi:10.1061/(ASCE)0733-9399(2008)134:5(385)

Mielniczuk, B., Hueckel, T., & El Youssoufi, M. S. (2014). Evaporation-induced evolution of the capillary force between two grains. *Granular Matter, 16*(5), 815-828. doi:10.1007/s10035-014-0512-6

Neuman, S. P. (2005). Trends, prospects and challenges in quantifying flow and transport through fractured rocks. *Hydrogeology Journal, 13*(1), 124-147.

Nitao, J. J., & Buscheck, T. A. (1991). Infiltration of a liquid front in an unsaturated, fractured porous medium. *Water Resources Research, 27*(8), 2099-2112.

Orr, F. M., Scriven, L. E., & Rivas, A. P. (1975). Pendular rings between solids - meniscus properties and capillary force. *Journal of Fluid Mechanics, 67*(FEB25), 723-742. doi:10.1017/S0022112075000572

Peters, R., & Klavetter, E. A. (1988). A continuum model for water movement in an unsaturated fractured rock mass. *Water Resources Research, 24*(3), 416-430.

Philip, J. R. (1957a). The theory of infiltration: 1. the infiltration equation and its solution. *Soil Science, 83*(5), 345-358.

Philip, J. R. (1957b). The theory of infiltration: 4. sorptivity and algebraic infiltration equations. *Soil Science, 84*(3), 257-264.

Press, W. H., Flannery, B. P., Teukolsky, S. A., & Vetterling, W. T. (1986). Numerical recipes: The art of scientific computing (cambridge.

Reinson, J. R., Fredlund, D. G., & Wilson, G. W. (2005). Unsaturated flow in coarse porous media. *Canadian Geotechnical Journal, 42*(1), 252-262.

Richards, L. A. (1931). CAPILLARY CONDUCTION OF LIQUIDS THROUGH POROUS MEDIUMS. *Journal of Applied Physics, 1*(5), 318-333. doi:http://dx.doi.org/10.1063/1.1745010

Saez, A., & Carbonell, R. (1987). The equilibrium shape and stability of menisci formed between two touching cylinders. *Journal of Fluid Mechanics, 176*, 357-378.

Saez, A., & Carbonell, R. (1990). The equilibrium and stability of menisci between touching spheres under the effect of gravity. *Journal of Colloid and Interface Science, 140*(2), 408-418. doi:10.1016/0021-9797(90)90361-Q

Schubert, C., Lindner, J., & Kelly, R. (1986). Experimental methods for measuring static liquid holdup in packed columns. *AIChE Journal, 32*(11), 1920-1923.

Seol, Y., Liu, H. H., & Bodvarsson, G. S. (2003). Effects of dry fractures on matrix diffusion in unsaturated fractured rocks. *Geophysical Research Letters, 30*(2)

Slobozhanin, L. A., Alexander, J. I. D., Collicott, S. H., & Gonzalez, S. R. (2006). Capillary pressure of a liquid in a layer of close-packed uniform spheres. *Physics of Fluids, 18*(8), 082104. doi:10.1063/1.2236123 ER

Takagi, D., & Huppert, H. E. (2010). Flow and instability of thin films on a cylinder and sphere. *Journal of Fluid Mechanics, 647*(March), 221-238.

Tidwell, V. C., Glass, R. J., & Peplinski, W. (1995). Laboratory investigation of matrix imbibition from a flowing fracture. *Geophysical Research Letters, 22*(11), 1405-1408.

Tokunaga, T. K., Olson, K. R., & Wan, J. (2005). Infiltration flux distributions in unsaturated rock deposits and their potential implications for fractured rock formations. *Geophysical Research Letters, 32*(5)

Tokunaga, T. K., & Wan, J. M. (2001). Approximate boundaries between different flow regimes in fractured rocks. *Water Resources Research, 37*(8), 2103-2111. doi:10.1029/2001WR000245

Tokunaga, T. K., & Wan, J. M. (1997). Water film flow along fracture surfaces of porous rock. *Water Resources Research, 33*(6), 1287-1295. doi:10.1029/97WR00473

Tokunaga, T. K. (2009). Hydraulic properties of adsorbed water films in unsaturated porous media. *Water Resources Research, 45*, W06415. doi:10.1029/2009WR007734

Tokunaga, T. K., Olson, K. R., & Wan, J. (2003). Moisture characteristics of hanford gravels: Bulk, grain-surface, and intragranular components. *Vadose Zone Journal, 2*(3), 322-329.

Tsang, C., Neretnieks, I., & Tsang, Y. (2015). Hydrologic issues associated with nuclear waste repositories. *Water Resources Research, 51*(9), 6923-6972.

Turner, G., & Hewitt, G. (1959). The amount of liquid held at the point of contact of spheres and the static liquid holdup in packed beds. *Trans.Instn.Chem.Engrs, 37*(6), 329-334.

Urrutia, G., Bonelli, P., Cassanello, M., & Cukierman, A. (1996). On dynamic liquid holdup determination by the drainage method. *Chemical Engineering Science, 51*(15), 3721-3726.

Wang, J. S. Y., & Narasimhan, T. N. (1985). Hydrologic mechanisms governing fluid-flow in a partially saturated, fractured, porous-medium. *Water Resources Research, 21*(12), 1861-1874. doi:10.1029/WR021i012p01861

Wheatcraft, S. W., & Winterberg, F. (1985). Steady state flow passing through a cylinder a permeability different from the surrounding medium. *Water Resources Research, 21*(12), 1923-1929. doi:http://dx.doi.org/10.1029/WR021i012p01923

Willett, C. D., Adams, M. J., Johnson, S. A., & Seville, J. P. (2000). Capillary bridges between two spherical bodies. *Langmuir, 16*(24), 9396-9405.

Wood, T. R., Glass, R. J., McJunkin, T. R., Podgorney, R. K., Laviolette, R. A., Noah, K. S., . . . Baker, K. (2004). Unsaturated flow through a small fracture-matrix network: Part 1. experimental observations. *Vadose Zone Journal, 3*(1), 90-100.

Xiao, Q., Anter, A., Cheng, Z., & Yuan, W. (2000). Correlations for dynamic liquid holdup under pulsing flow in a trickle-bed reactor. *Chemical Engineering Journal, 78*(2), 125-129.

Youngs, E. G. (2008). Steady water flow through unsaturated aggregated porous materials. *Transport in Porous Media, 71*(2), 147-159. doi:10.1007/s11242-007-9116-5

Youngs, E. G., & Kacimov, A. R. (2007). Conduction through an assembly of spherical particles at low liquid contents. *International Journal of Heat and Mass Transfer, 50*(1–2), 292-302. doi:http://dx.doi.org/10.1016/j.ijheatmasstransfer.2006.06.006

Zimmerman, R. W., Bodvarsson, G. S., & Kwicklis, E. M. (1990). Absorption of water into porous blocks of various shapes and sizes. *Water Resour.Res, 26*(11), 2797-2806.

CURRICULUM VITAE

Jeevan A. Jayakody

Department of Geoscience, University of Nevada, Las Vegas

4505 S Maryland Parkway, Las Vegas, NV 89154

jayakody@unlv.nevada.edu

EDUCATION

Ph.D in Geoscience, University of Nevada Las Vegas (expected graduation May 2016)

M.S. in Geoscience, University of Nevada Las Vegas, 2010

B.S. in Geology, University of Peradeniya, Sri Lanka, 2005

EMPLOYMENT

01/2008 – Present	Graduate Assistant, Department of Geoscience, University of Nevada, Las Vegas
04/2006 – 12/2007	Hydrogeologist, CH2M HILL - USAID Sri Lanka Tsunami Reconstruction Program
10/2005 – 04/2006	Lecturer, Department of Geology, University of Peradeniya, Sri Lanka
06/2005 – 10/2005	Research Assistant, Postgraduate Institute of Science, Univ. of Peradeniya, Sri Lanka

PUBLICATIONS

Jayakody, J.A., and Nicholl, M.J., Influence of hydraulic bridges on flow within a coarse porous clast. (submitted to Advances in Water Resources)

Jayakody, J.A., Nicholl M.J., and Simon, A.C. (2011). Spatial and temporal structure of unsaturated flow in porous crushed stone. Proceedings of the 43rd Symposium on Engineering geology and Geotechnical Engineering, Las Vegas, NV

Jayakody, J.A. (2010). Characterization of unsaturated flow in dual-porosity granular media, M.S. Thesis, University of Nevada, Las Vegas (unpublished)

Jayakody, J.A. (2005). Investigation of Nortonbridge Reservoir leakage, Sri Lanka, B.S. thesis, University of Peradeniya, Sri Lanka (unpublished)